NASA Contractor Report 174870

A Study of the Stress Wave Factor Technique for the Characterization of Composite Materials

A.K. Govada, J.C. Duke, Jr., E.G. Henneke II, and W.W. Stinchcomb

Virginia Polytechnic Institute and State University
Blacksburg, Virginia 24061

February 1985

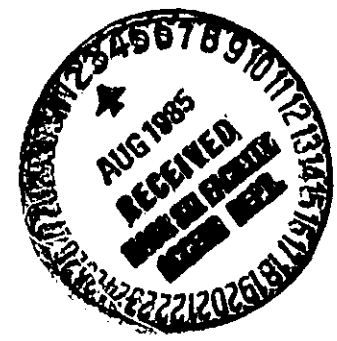

Prepared for

NATIONAL AERONAUTICS AND SPACE ADMINISTRATION
Lewis Research Center
Under Grant NAG 3-172

A Study of the Stress Wave Factor Technique for the Characterization of Composite Materials

(ABSTRACT)

This study has investigated the potential of the Stress Wave Factor as an NDT technique for thin composite laminates. The conventional SWF and an alternate method for quantifying the SWF were investigated.

Agreement between the initial SWF number, ultrasonic C-scan, in-plane displacements as obtained by full field moire interferometry, and the failure location have been observed. The SWF number was observed to be the highest when measured along the fiber direction and the lowest when measured across the fibers. The alternate method for quantifying the SWF used square root of the zeroth moment ($\sqrt{M_0}$) of the frequency spectrum of the received signal as a quantitative parameter. When $[0,90_2]_s$, $[0,\pm45]_s$ and $[0,90,\pm45]_s$ graphite epoxy laminates were cyclically loaded, $\sqrt{M_0}$ decreased with the number of cycles. Decreases in the amplitudes of the higher harmonics of the frequency spectrum occurred as a result of transverse matrix cracking in the 90° plies of the laminates. The decreases in $\sqrt{M_0}$ were in agreement with the reduction in laminate stiffness due to cyclic loading. The decreases in $\sqrt{M_0}$ were larger than the reduction in the laminate stiffnesses due to cyclic loading.

From this study it therefore appears that the stress wave factor has an excellent potential to monitor damage development in thin composite laminates.

TABLE OF CONTENTS

	Page
ABSTRACT	i
1. INTRODUCTION	1
1.1 Scope	1
1.2 Background	2
1.3 Objectives	5
2. EXPERIMENTS AND RESULTS	7
2.1 Phase I	7
2.1.1 Reproducibility of the SWF number	7
2.1.2 Correlation of SWF with Failure Location	9
2.1.3 Correlation of SWF with Other NDT Techniques	11
2.1.4 Variation of the SWF with Fiber Orientation	14
2.1.5 Effect of the number of plies on the SWF	15
2.2 Phase II	15
2.2.1 An Alternate Method to Quantify the SWF	16
2.2.2 Correlation of the Root Mean Square of the Frequency Spectrum with the Laminate Stiffness During Fatigue	18
2.3 Phase III	21
2.3.1 Computer Code to Calculate Various Moments of the Frequency Spectrum	22

2.3.2 Flow Chart of the Data Acquisition, FFT, and Root Mean Square Evaluation System 22

3. DISCUSSION AND SUMMARY 23

3.1 Initial Investigation 25

3.2 Frequency Analysis 26

3.3 Usefulness of the SWF as an NDT Technique 31

4. CONCLUSIONS 33

5. REFERENCES 93

6. APPENDICES

6.1 Appendix A 95

6.2 Appendix B 98

1. INTRODUCTION

1.1 Scope

The use of fiber-reinforced composite materials has become increasingly popular for a wide range of applications, especially for high performance structures. Two of the primary advantages of composite materials are that they have high strength to weight and high stiffness to weight ratios. Also, the direction dependent properties of composites can be utilized in a number of applications. In order to use these materials effectively in engineering design one needs to understand:

- how these materials behave under load.
- the effects of initial imperfections on the final properties,
- the nature of damage development under load,
- the sequence of damage events that lead to the final fracture,
- and the effect of damage on the remaining strength, stiffness and/or life of the material.

Nondestructive testing (NDT) and evaluation of composite materials have received increasing attention in recent years to evaluate and predict the mechanical properties of the material in both the as-received condition and during service loading. Composite materials develop a complex state of damage when subjected to load [1,2]. Damage in these materials usually includes a combination of the following: matrix cracks, micro delamination, macro delamination, fiber splits, debonding, fiber breaks, etc. Because of this complex damage state conventional NDT methods are unable to provide a useful parameter to characterize this damage. There is, therefore, a strong need to develop

an NDT technique which is capable of yielding a parameter which is indicative of the total damage in the material. The ultrasonic Stress Wave Factor (SWF) is one such technique. The SWF technique was developed by Vary and his co-workers [3].

The SWF technique has the potential to inspect and interrogate the state of damage in a material. As will be seen in section 1.2, ultrasound beams interact with the entire volume of the material through which they travel. Therefore their propagation will be affected by the total damage state that lies in their path. A brief review of the work done in recent years in the areas of ultrasonic and acousto-ultrasonic NDT techniques is presented in the next section.

1.2 Background

Ultrasonic and more recently acousto-ultrasonic NDT techniques have become increasingly popular to detect damage and strength variations in fiber-reinforced composite materials. It has been reported [4] that from the measurement of extensional and shear moduli elastic and strength properties can be empirically evaluated. It has also been shown that ultrasonic attenuation in composites is sensitive to features (microvoids, etc.) that influence strength properties [5].

It has been shown that stress wave propagation is pivotal during failure of composites [6,7,8,9]. The SWF is an acousto-ultrasonic NDT technique. A schematic of the SWF set-up is shown in Fig. 1 [10]. A repeated series of ultrasonic pulses are injected into the specimen by means of a sending transducer. Each of these pulses simulates acoustic emission events in the material [19,20]. A separate receiving

transducer on the same side of the specimen intercepts some of the stress wave energy that radiates from the point of injection. The signals arriving at the receiving transducer resemble burst type acoustic emission events [21]. The degree of attenuation of the ultrasonic wave as it travels through the specimen is converted to a numerical value called the Stress Wave Factor (SWF) after appropriate signal conditioning. Vary et al. [3] define the SWF as the product of the number of times the voltage level of a single signal exceeds a set threshold level, the pulse repetition rate, and a predetermined length of time before the counter is reset. This is schematically shown in Fig. 2.

$$SWF = C\ T\ \frac{1}{p} \tag{1}$$

where

C = total number of counts of a single signal that exceeds a set threshold level.

T = time before the counter is reset.

$\frac{1}{p}$ = pulse repetition rate.

Vary et al. [3] describe the SWF as a measure of stress wave energy transmission. Their hypothesis was that decreased stress wave energy flow corresponds to decreased fracture resistance. The SWF provides a means of rating the efficiency of dynamic strain energy transfer in a given material. If the material exhibits an efficient stress wave energy transfer, then it will have higher strength. That is, better stress wave transmission means better transmission of dynamic stress and load distribution. Conversely, low values of SWF would indicate places

where the dynamic strain energy is likely to concentrate and promote fracture. Higher attenuation gives rise to a lower SWF. In other words, the higher the SWF, the less the attenuation of stress waves. Therefore, the SWF can be used as an NDT technique. A composite with high values of SWF would therefore exhibit higher strength locally because the stress wave dissipation of energy is enhanced by the same features that increase SWF. Conversely, low values of SWF would indicate that strain energy is likely to concentrate near crack nucleation sites and induce crack growth [10].

It has been shown that the SWF decreases in proportion to fractional powers of the ultimate strength and that it may be a useful aid in predicting failure locations in thin graphite epoxy laminates [3]. The SWF was found to be a sensitive indicator of composite strength variations that accompany various fiber orientations relative to the load axis. SWF was also found to be sensitive to strength variations in composite laminates because of variations in the cure pressures [11]. The SWF was also found to correlate strongly with interlaminar shear strength of graphite polyimide composite laminates [12]. Strong correlation between the SWF and an index of fracture toughness was reported by Hull et al. [13]. Williams et al. [14] reported that correlations exist between drop weight impacts, residual strength, through thickness attenuation and the SWF for graphite epoxy laminates that were subjected to repeated controlled low velocity drop weight impacts in the laminate direction. Henneke et al. [15] have shown that SWF can predict failure location in thin E-glass epoxy laminates. Govada et al. [16] reported that ultrasonic attenuation and

the SWF were sensitive to damage development in metal matrix composites. Duke et al. [17] reported that the SWF correlated well with the reduction in stiffness during fatigue loading of graphite epoxy composite laminates. Hayford et al. [18] have shown that delamination and matrix cracking in graphite epoxy specimens can be detected by measuring the amplitude attenuation of an ultrasonic pulse propagated through the laminate thickness using a pulse-echo method.

It is therefore clear that ultrasonic and acousto-ultrasonic techniques can be used to interrogate and assess damage, and predict mechanical properties of composite materials. In this study the potential for the ultrasonic Stress Wave Factor as an NDT technique to assess damage and predict mechanical properties of composite materials is investigated. The objectives of this study are listed in the next section.

1.3 Objectives

The objectives of this study are divided into three phases.

Phase I:
a) Determine the feasibility of the SWF technique as a potential NDT method for fiber-reinforced composite materials.
b) Check the validity of the SWF results using other NDT techniques.

Phase II:
a) Investigate an alternate method (shape parameters of the Fourier Transform of the acousto-ultrasonic signal) to quantify the SWF technique and thereby eliminate the need for a threshold level and

several other instrumentation and experimental parameters.

b) Apply the alternate method to fiber-reinforced composite laminates subjected to cyclic loading and correlate the degradation of stiffness, due to damage, to the root mean square value of the frequency spectrum.

Phase III: Develop a computer code which can calculate various moments of the Fourier Transform of the received signal.

2. EXPERIMENTS AND RESULTS

2.1 Phase I

In the initial phase of the feasibility study of the SWF as an NDT technique, a commercial instrument, AET model 206AU*, was used, Fig. 3. This instrument contains a pulser, a receiver, a transmitter-receiver transducer assembly, an oscilloscope to display the received signal, and a counter. The specimens used were E-glass epoxy composite laminates with various stacking sequences.

2.1.1 Reproducibility of the SWF Number

For making an SWF measurement, two transducers, a transmitter and a receiver, must be applied to the specimen. In order to mount the transducers to the specimen one needs to consider the pressure applied to the transducers, the type and amount of couplant used between the transducer and the specimen, and the surface finish of the specimen.

In order to obtain a constant reading of the SWF, it was found to be necessary to apply at least 2 lbs. load on each transducer. The value of the SWF decreased slightly with increase in load up to about 20 lbs. on each transducer wherefore it remained constant. For loads greater than 20 lbs. on each transducer, some surface damage was noticed on the specimen. A value of 15 lbs. on each transducer was chosen, as

---

* Acoustic Emission Technology Corporation
1812J Tribute Road
Sacramento, CA 95815

this value did not damage the specimen and the SWF number was sufficiencly high, remained constant, and was easily reproduced.

The various couplants used, in order of increasing viscosity, were Nonaq stopcock grease, Ultragel couplant, Dow-Corning silicone grease, and Panametrics shear wave couplant. Panametric couplant, which has the highest viscosity, provided the highest SWF for glass epoxy specimens. For all the subsequent work in this study, Panametrics couplant was used. The amount of couplant did not significantly affect the SWF values or its reproducibility.

The surface irregularities on the specimen due to the scrim cloth used in the processing procedure did not significantly affect the SWF values when compared with those of a polished specimen.

Some general observations regarding the instrumentation must be noted: for lower repetition rates of the input pulse there is a smaller scatter in the SWF values. Also, smaller scatter is obtained at higher threshold levels and narrower gate widths. Figure 4 is the schematic representation of the interrelationship between signal, threshold, and gate width. If the threshold is set too high and/or the gate too narrow, some of the useful excursions in the signal may not be included in the SWF number. On the other hand, if the threshold is too low, the counter will detect some of the noise associated with the signal and if the gate is too wide it will cause the counter to detect some higher level noise at the tail end of the signal. Therefore a trade-off must be made. To obtain meaningful SWF values one must observe the shape of the signal and then choose the instrumentation parameters accordingly. The parameters chosen must yield reproducible SWF values. After

systematic testing and evaluation, the following instrumentation and experimental parameters were found to provide reproducible SWF values to within ±10 % for glass epoxy laminates.

Threshold level:	1.00 volt
Threshold mode:	auto (eliminates some of the noise from the counting circuits
Gate:	4 units
Trigger rate:	0.5 kHz
Gain:	45 dB
Sweep rate:	62.5 μsec/division
Couplant:	Panametrics shear couplant
Pressure on each transducer:	15 lbs.
Distance between the transducers:	1.5 inches

Several instrumentation difficulties had to be overcome before the SWF measurements were made to be reproducible [15]. The difficulties will not be further reported here.

2.1.2 Correlation of SWF with Failure Location

A large number of tensile specimens were tested for the initial SWF number. These specimens were then loaded in quasi-static tension to failure. In general, the outcome of this testing showed that there is a correlation between the initial SWF number and the final failure location in the composite laminates. To determine this correlation, one

must exercise extreme care when selecting the instrumentation and experimental parameters to measure the SWF. The parameters listed in section 2.1.1 were used for this test program.

The specimens tested were E-glass epoxy composite laminates. The dimensions of the specimens were 1.0" by 8.0" long. Several different stacking sequences were investigated. Measurements of the SWF were made along the length of the specimen at 0.25" intervals. A schematic of the measurement pattern is shown in Fig. 6. Panametrics shear wave couplant was used. A load of 30 lbs. was applied on the transducer assembly by means of a spring loading frame, Fig. 3. At each location on the specimen, ten individual measurements of the SWF were made. After each measurement the transducers were removed from the specimen, the couplant was wiped off, fresh couplant was applied, and a new measurement at the same location was made. After the measurements were made, an average value of the SWF was determined for each location on the specimen. The variation of these values was within 10%. The SWF values for the various positions on the specimen were plotted. Figure 7 shows a typical normalized SWF versus position plot for a $[0,90_3]_s$ E-glass laminate. Normalizing was done with respect to the maximum SWF value. Because of the nature of the measurement of the SWF, there is an overlap of values. To eliminate any shift in the data because of this overlap, the SWF values can be averaged. A comparison of an averaged normalized SWF plot and an unaveraged normalized SWF plot is shown in Fig. 8. The distance between the transducers is 1.5". Each measurement interval is 0.25". The averaging is done by taking the sum of seven numbers, three

on either side of the location one wants to calculate the average SWF value, and take the mean.

The specimens were then loaded in quasi-static tension until they fractured. The loading was done on an MTS servo-hydraulic, closed-loop testing frame. A schematic of each of the specimens indicating the fracture, by a shaded area, was then put beneath the appropriate normalized SWF versus position plot. This would allow one to check for correlation between the lowest value of the SWF and the fracture location on the specimen. Figure 9 shows one such plot for a $[0,90_3]_s$ E-glass laminate. From Fig. 9 one can clearly observe that there is indeed a correlation between the lowest value of the SWF and the fracture location on the specimen. Figures 10 through 13 show similar correlations for various other stacking sequences for E-glass epoxy laminates. One should note at this point that these correlations are valid only for a given set of parameters. For example, if the threshold were different, a different fracture location might have been predicted. An alternate method to quantify the SWF will be discussed in section 2.2.1 where the need for selecting a threshold level and several other instrumentation parameters is eliminated.

2.1.3 Correlation of SWF with Other NDT Techniques

In the previous section, SWF demonstrated that it has the potential to predict failure locations on glass epoxy laminates nondestructively. To explore further the significance of the SWF values, various other NDT techniques such as moiré interferometry, X-ray radiography, ultrasonic C-scan, edge replication, etc. were applied to

the specimens that have been evaluated by the SWF. Of these techniques, moiré interferometry and ultrasonic C-scan appeared to provide additional insight concerning the SWF measurements.

A total of three $[0,90_3]_s$ E-glass epoxy laminates were tested in this program. On each of the specimens the following tests were performed:

- evaluation of the SWF along the length of the specimen,
- ultrasonic C-scanning of the specimen,
- calculation of the local stiffness, from the in-plane displacement (u) field as obtained by full field moiré interferometry of the specimen.

After these tests were made on the specimens, the results were analyzed and correlations, if any, were observed. The specimens were then loaded in quasi-static tension until final fracture. The fracture regions were checked with the locations predicted by the SWF. In this study, results from one specimen are presented.

This specimen was 1.0" x 7.0" long. SWF was measured along the length of the specimen. Figure 7 shows a plot of the normalized SWF versus the position on the specimen. From Fig. 7 one can observe that the top end, center, and the bottom end of the specimen had low SWF values. Figure 14 shows the ultrasonic C-scan of the specimen. Note the indication of flaws at the top end, center, and the bottom end of the specimen. The specimen was then studied in a moiré interferometry set-up so that the u displacement field was obtained. Appendix A describes the moiré interferometry technique [22]. A grating of 30,000 lines/inch was glued to the specimen so that the furrows on the grating

were along the longitudinal axis of the specimen. The frequency of the virtual grating was 60,000 lines/inch. The effective field was about 1.0" x 3.75". The field size is limited by the size of the lenses. Since the specimen under study had a gage length of 4.0", a field of 1.0" x 3.75" was adequate. The specimen was then fixed in the loading frame of the moiré interferometric set-up and loaded to various values of strain. Figure 15 shows the u displacement field at 500 με which corresponds to about 100 lbs. load. At this low level of strain the moiré fringes are uniformly spaced, indicating uniform displacement field along the length of the specimen. Figure 16 shows the u displacement field at 2000 με which corresponds to about 400 lbs. load. Here the moiré fringes are nonuniform along the length of the specimen. From the displacement contours in Fig. 16 local strains were calculated. As the applied axial load was constant local stiffness from the local strains were calculated along the length of the specimen. Figure 17 shows a plot of the relative local stiffness and normalized SWF values versus the position on the specimen. From the local stiffness plot in Fig. 17 one can see that the top end, center, and the bottom end of the specimen had lower stiffnesses compared to other regions. Comparing Figs. 14 and 17, there appears to be a trend between the SWF values, ultrasonic C-scan, and the local stiffness of the specimen. The areas of low SWF values corresponded with the "white" areas of the C-scan and areas of high displacement in the moiré fringe pattern.

The specimen, after being removed from the load frame of the moiré interferometric set-up, was pulled in quasi-static tension until final

fracture. The specimen failed in the top grip. As a result, one cannot make meaningful correlations between fracture, the local stiffness, and the SWF values for this specimen. The interpretation of failure in the grip region is complicated because of the complex state of stress caused by the grips. However, it is interesting to note that the fractured region had low values of SWF and local stiffness (see Fig. 17). The other two glass epoxy laminates did fail in the vicinity of the predicted locations and in between the grips. Results of the specimen that fractured in the grip were used because the photographs of the moiré fringes had the best contrast. Therefore, visualizing the areas of high and low strains is relatively easy.

2.1.4 Variation of the SWF with Fiber Orientation

To evaluate the effect of the variation in the SWF with fiber orientation, three panels: $[0]_8$ graphite epoxy, $[0]_8$ S-glass epoxy, and random fiber S-glass epoxy laminates were utilized in this study. Each of the panels was approximately 12 in. by 12 in. The thicknesses of the laminates were in the range 0.045 - 0.051 in. Figure 18 shows the schematic of the measurement pattern utilized. The sending transducer was placed in the center of the panel and the receiving transducer was moved around the sending transducer as a function of the fiber orientation. The instrumentation parameters listed in 2.1.1 were used here. Figure 19 shows the variation of the SWF with fiber orientation for a $[0]_8$ graphite epoxy laminate. Figure 20 shows the variation of the SWF with fiber orientation for a $[0]_8$ S-glass epoxy laminate. Note that in both cases the SWF is the maximum along the fiber direction and

minimum across the fibers. Figure 21 shows the variation of SWF in an arbitrarily chosen 0° to 90° gradient of the random fiber S-glass epoxy panel. Note that the SWF is approximately constant.

2.1.5 Effect of the Number of Plies on the SWF

Since the sending and the receiving transducers are on the same side of the specimen, it is likely that the acousto-ultrasonic signal is representative only of the top few plies of the laminate. A simple experiment was performed to evaluate how many plies the SWF technique interrogates. Figure 22a shows a schematic of an edge replica of a $[0,90_2,0]_s$ graphite epoxy specimen. Figures 22b and 22c show the signal on side A and side B for this specimen. The specimen was then bent to introduce matrix cracks in the 90° plies towards side B as shown by the schematic of an edge replica in Fig. 23a. The signal corresponding to side A is shown in Fig. 23b. Note that there is not much change in the signal amplitude when compared with Fig. 22b. However, the amplitude of the signal corresponding to side B, Fig. 23c, decreased significantly when compared with that of Fig. 22c. This indicates that the SWF technique interrogates only the first 3-4 plies of the laminate.

2.2 Phase II

In section 2.1.1, instrumentation and experimental parameters were listed which produced reproducible SWF values to within ±10%. In section 2.1.2, correlations between the SWF and the fracture location on E-glass epoxy laminates were discussed. The correlations were found to hold only for the particular set of parameters listed in section 2.1.1.

Results are especially sensitive to the threshold level. In order to eliminate the need for the threshold level and most other instrumentation and experimental parameters, an alternative method to quantify the SWF was investigated. This method is discussed in detail in the following section.

2.2.1 An Alternate Method for Quantifying the SWF

A schematic of the experimental set-up for this method is shown in Fig. 24. Two transducers, one acting as a transmitter, the other as a receiver, were mounted on the same side of the specimen as shown. The transducers were matched broadband transducers, 0.5" in diameter and had a center frequency at nominally 5 mHz. The transducers were Panametric model V109. Panametrics shear wave couplant was used between the transducers and the specimen. The transducers were held in a plexiglass fixture so that the distance between their centers was fixed at 1.0". A pair of elastic bands at each end of the plexiglass fixture kept the transducer assembly from sliding downthe specimen. A Panametrics model 5052A was used as a pulser/receiver. A Panametrics model 5050AE preamplifier was used to amplify the received signal. A transient waveform recorder, Biomation model 8100, was used to digitize the signal. A Fast Fourier Transform algorithm was used to perform the spectral analysis of the signal. A typical signal and its frequency spectrum for an undamaged $[0,90_2]_s$ graphite epoxy laminate is shown in Fig. 25. Talreja [23] has noted that three classes of paremeters are needed to describe the distribution functions, namely location, scale and shape parameters. He suggested that a convenient set of parameters

to represent a frequency spectrum can be defined by considering the spectrum to be a plane figure closed on the frequency axis. The location parameter for the frequency spectrum can then be taken to be the location of the centroid of this figure. The area of this figure forms a suitable scale parameter and the shape parameters can be described in terms of the various moments of the figure about a convenient axis. Talreja therefore proposed that a set of shape parameters be defined by

$$S_{r,k} = \frac{M_r}{M_{r-k}\, f_c^{\,k}} \qquad \begin{array}{l} k = 1,2,3\ldots \\ r = 2,3,4\ldots \\ r > k \end{array}$$

where

$$M_r = \int_{-\infty}^{\infty} S(f)\, f^r d\, f$$

where $S(f)$ is the power spectral density, f is the frequency, and f_c is the location of the centroid found by the following expression

$$f_c = \left(\frac{M_1}{M_0}\right)$$

Several of the moments and moment ratios can be given physical interpretations. For example, M_0 is the mean square value of the power spectral density. Also,

$$f_0 = \left(\frac{M_2}{M_0}\right)^{1/2}$$

is the frequency of mean value crossings with positive slopes and

$$f_p = \left(\frac{M_4}{M_2}\right)^{1/2}$$

is the frequency of maxima in the time domain [24]. In this study the root mean square of the power spectral density, $(M_0)^{1/2}$, was used as the parameter for the alternate method to quantify SWF. In applying this technique the need for the threshold level and several other instrumentation parameters is eliminated. The only instrumentation parameter used was the gate width. The gate width was chosen so that only the initial part of the signal was received by the transient wave form recorder.

2.2.2 Correlation of the Root Mean Square of the Frequency Spectrum with the Laminate Stiffness During Fatigue

A schematic diagram of the experimental set-up is shown in Fig. 24. The specimens tested were T-300/5208 graphite epoxy laminates measuring 1.0 in. by 8.0 in. long. Three stacking sequences were investigated: $[0,90_2]_s$, $[0,\pm45]_s$ and $[0,90,\pm45]_s$. The ends of the specimens, approximately 1.5 in., were coated with a thin uniform layer of MS907 epoxy manufactured by Miller-Stephenson Chemical Company. This coating provided a uniform gripping surface. Two thicknesses of 320 grit emery paper were inserted between the MTS grips and the specimen during fatigue loading to improve the gripping efficiency. The cyclic loading was done on an MTS servo-hydraulic, closed-loop testing frame. Stiffness was measured by means of an extensometer attached to the center portion of one side of the specimen. The extensometer gage

length was nominally 2 in. The extensometer knife edges sat in V-shaped grooves machined into aluminum tabs. These tabs were bonded to the specimen by means of RTV silicone rubber cement manufactured by 3-M Company. On the other side of the specimen, the transducer assemply discussed in section 2.2.1 was attached. The transducer assembly was positioned so that it was at the center of the specimen directly opposite the extensometer.

The fatigue tests were conducted at a constant stress ratio, R=0.1, in a sinusoidal form at a cyclic frequency of 10 Hz in a tension-tension mode. The maximum stress amplitudes used for the testing [2] were as follows:

$[0,90_2]_s$, $\sigma_{max} = 0.70\ S_{ult}$

$[0,\pm45]_s$, $\sigma_{max} = 0.72\ S_{ult}$

$[0,90,\pm45]_s$, $\sigma_{max} = 0.62\ S_{ult}$

where S_{ult} is the ultimate tensile strength. The pulser transmits ultrasonic pulses through the sending transducer. The ultrasonic signal was picked up by the receiving trandsucer. The signal was sent through a preamplifier and then an amplifier. A filtering circuit was used to filter out frequencies less than 100 kHz. This removed any noise associated with the MTS hydraulic system. An oscilloscope was used to display the signal. The signal was then fed into a counter where the counts above a certain threshold were calculated (conventional SWF). The signal was also captured and digitized using a transient waveform recorder. The signal was stored on a floppy disk of a Z-80 based microprocessor. A Fast Fourier Transform algorithm was used to generate

the frequency spectrum of the signal. Root mean square of the frequency spectrum (also called power spectral density) was calculated from the spectrum.

Results from a typical $[0,90_2]_s$ graphite epoxy specimen are presented next. The letter N shall be used to denote the number of cycles, and P, the load. The specimen was inserted into the grips of the MTS machine and all the necessary attachments were made to obtain the signal and the stiffness. Figure 26 shows the signal and the frequency spectrum at N=0 and P=0. Note the presence of two harmonic frequencies, one centered approximately at 300 kHz and the other centered approximately at 750 kHz. Figure 27 shows the signal and the frequency spectrum for N=$\frac{1}{2}$, P=mean load, 1248 lbs. Note the reduction in the higher harmonic frequencies. Figures 28 through 34 show the signals and their corresponding frequency spectra for various numbers of cycles and at P=mean load, throughout the fatigue life of the specimen. In all cases signals and stiffnesses were recorded at mean load with the cycling stopped. Root mean square values of the spectra were then calculated. Table 1 shows the root mean square values and the stiffnesses for this specimen. Figure 35 shows the stiffness and the root mean square value versus the number of cycles. Note the correlation between the stiffness and the root mean square values of the frequency spectra. Figure 36 shows a plot of fp versus strain for $[0,90_2]_s$ laminate. Figure 37 shows a plot of fc and fo versus strain for $[0,90_2]_s$ laminate. Figure 38 shows penetrant-enhanced X-ray radiographs of $[0,90_2]_s$ graphite epoxy laminate at 60,000 cycles and 100,000 cycles.

Figures 39 through 45 show the signals and the corresponding frequency spectra for various number of cycles for a $[0,\pm45]_s$ graphite epoxy laminate. Figure 46 shows the plot of stiffness and the root mean square values versus the number of cycles for $[0,\pm45]_s$ laminate. Note the correlation between the stiffness and the root mean square values of the frequency spectra.

Figures 47 through 51 show the signals and the frequency spectra for various number of cycles for a $[0,90,\pm45]_s$ laminate. Figure 52 shows the plot of stiffness and the root mean square values versus the number of cycles for $[0,90,\pm45]_s$ laminate. Note the correlation between the stiffness and the root mean square values of the frequency spectra.

2.3 Phase III

In section 2.2.2, correlations between the root mean square of the frequency spectrum and the stiffness reduction during fatigue were shown. The root mean square values of each of the spectra were calculated manually. The number of signals and their spectra would get large for long-term fatigue tests. To decrease the computation time necessary to calculate the root mean square values, a computer code was written. The quantities that the program calculates are $(M_0)^{1/2}$, (M_1/M_0), $(M_2/M_0)^{1/2}$, $(M_4/M_2)^{1/2}$. Section 2.2.1 describes these ratios in detail.

2.3.1 Computer Code to Calculate Various Moments of the Frequency Spectrum

A pulser sends ultrasonic pulses through the specimen by means of a sending transducer. The signal received by the receiving transducer is preamplified, amplified, and after appropriate signal conditioning, is sent to a transient waveform recorder where the signal is digitized into 2048 points and stored. The data is then sent through a parallel I/O that is 8 bits wide, to a microprocessor. From the microprocessor the data is sent through a serial I/O and a modem to an IBM 370 mainframe computer for storage on disk. The entire process of sending a pulse through the specimen to storing the signal on disk takes about 50 seconds. An IMSL [25] subroutine was used to calculate the Fast Fourier Transform of the signal. To calculate the various moments of the frequency spectrum, a computer code was developed. Appendix B has the computer program.

2.3.2 Flow Chart of the Data Acquisition, FFT, and the Moments Evaluation System.

The flow chart for the system to capture the signal, transformation to the frequency domain, and calculation of the moments of the frequency spectrum is shown in Fig. 53.

3. DISCUSSION AND SUMMARY

This study has investigated the use of stress wave factor as a NDT technique for thin composite laminates. For the SWF to be a useful NDT technique, it must possess the following requirements:

- provide reproducible results
- should have very few experimental and instrumentation parameters
- should be easy to operate
- should be operator insensitive
- the results achieved by the technique should have the potential to be quantified
- the results should provide insight into the nature of damage development
- the technique should be able to yield a parameter that is indicative of the total damage between the transducers
- this parameter should be able to correlate/predict mechanical behavior
- the technique should have the capability of automatic inspection

From the results presented in the previous chapter, most of the above requirements appear to have been met. The technique provides reproducible results, is easy to operate, is operator insensitive, provides quantitative parameters, and provides some insight into the nature of damage development in composite laminates. Additional work needs to be done before one can be able to relate the quantitative

parameters obtained by this technique with the mechanical response of the material. However, a description of the nature of wave propagation is difficult because of the anisotropy of the composite laminates and the complex damage state that develops as a result of mechanical loading. When a mechanical wave propagates through a material it undergoes reflections, mode conversions, several attenuation mechanisms, dispersion, etc. Any variation in the material condition will generally cause a change in one or more of the above areas. A precise description of the material's condition is not possible using these concepts. If one were to have a precise description of the material's condition then the description will at best facilitate determination of the stiffness since the strength or life depend on the nature and history of the applied loads. In a large structure, determining the material condition everywhere is impractical. It is therefore desirable to determine where the material condition is "poor". Knowing this, attention can then be directed to determine the exact condition. It appears that the SWF technique as applied in this study possesses a tremendous potential for doing just this type of inspection.

The results presented in the previous chapter will be discussed in three sections. Section 3.1 deals with the initial phases of the investigation which includes reproducibility, failure location prediction, correlation with other NDT techniques, effect of fiber orientation on the SWF, effect of the laminate thickness on the SWF, and the nature of wave propagation. Section 3.2 discusses the frequency analysis and the correlation of the root mean square values to the laminate stiffness and damage development during cyclic loading.

Section 3.3 discusses the usefulness of the SWF as an NDT technique, advantages and limitations of the SWF.

3.1 Initial Investigation

For any NDT technique to be useful, it must be able to provide reproducible results. Using the AET model 206AU, several carefully monitored experiments were conducted on E-glass epoxy laminates. The outcome of these experiments was a set of parameters that yielded reproducible SWF values to within ±10% (see section 2.1.1). The variation of the SWF values by as much as 10% is due to the inability to place the transducers in the same location on the specimen, variation in the amount of couplant used, effects of temperature and moisture, and misalignment of the transducers relative to the specimen.

When virgin E-glass epoxy laminates wre evaluated by the SWF and then pulled in quasi-static tension, the specimens failed in the regions where the SWF was the lowest. This behavior suggests that areas of low SWF would be indicative of areas with poor stress wave energy transmission, thereby dynamic strain energy is likely to concentrate in such areas and promote failure. Local stiffnesses calculated from full field moire interferometry correlated well with SWF for E-glass laminates. This suggests that the local inhomogeneities present in the laminate that cause variations in mechanical properties also influence the stress wave propagation and hence the SWF. Ultrasonic C-scans of E-glass laminates were found to complement the SWF results. It is interesting to note that in the limiting case where a single transducer

is used as a sender and a receiver the SWF technique becomes the conventional pulse-echo A-scan.

The SWF was found to be sensitive to the fiber direction of the composite laminate. When unidirectional, 8-ply graphite epoxy and S-glass epoxy laminates were evaluated by the SWF, the SWF values were found to be the largest along the fiber direction and the smallest perpendicular to the fiber direction. This behavior suggests that the 0° plies transmit the stress wave energy more efficiently compared with 90° plies. It appears, therefore, that fiber orientation is critical not only to sustaining static loading but also to dynamic stress wave transmission.

A sequence of tests performed on $[0,90_2,0]_s$ graphite epoxy laminates have shown that the SWF obtains information mostly from the first four plies of the laminate.

3.2 Frequency Analysis

To eliminate the need for several experimental and instrumentation parameters, listed in section 2.1.2, the root mean square of the frequency spectrum of the received signal was investigated as an alternative method for quantifying the SWF, rather than counts above an arbitrary threshold level. This method has better sensitivity and is more practical to use than the conventional SWF. Figure 31 shows a signal and its spectrum for a $[0,90]_2$ graphite epoxy laminate that has been cycled to 30,000 cycles. The SWF is 787 and the $\left(\frac{M_o^N}{M_o^o}\right)^{1/2}$ is 0.68.

Figure 32 shows the signal and its spectrum for the same specimen at 95,000 cycles. Note that there is little change in the signal. The SWF is 790 while the $\left(\frac{M_o^{N\,1/2}}{M_o^o}\right)$ is 0.61. It has been shown [1] that for this type of laminate and test conditions there is a significant growth of micro-delamination from around 30,000 cycles to 100,000 cycles. The root mean square of the frequency spectrum is therefore more sensitive to damage than the conventional SWF. It is also more useful because a great deal of information is obtained about the signal from the frequency spectrum. One can obtain the root mean square value, the approximate frequency of mean zero value crossings with positive slopes, the approximate frequency of the maxima in the time domain and the centroid of the frequency spectrum (see section 2.2.1). The results presented in section 2.2.2 show that the root mean square values of the frequency spectrum correlate extremely well with the reduction in laminate stiffness during cyclic loading. Three different stacking sequences of graphite epoxy laminates were tested. Results from each of these stacking sequences is discussed next.

$[0,90_2]_s$ Laminate

Figure 26 shows the signal and its frequency spectrum of the specimen at N=0 and P=0. Note the presence of two harmonic frequencies, one centered at approximately 250 kHz and the other centered at approximately 750 kHz. Figure 21 corresponds to N=$\frac{1}{2}$ and P=mean load=1238 lbs. The amplitudes of the second harmonic frequencies are

reduced. It has been shown [2] for the test conditions used, transverse cracks in the 90° plies appear at this load level. Therefore the transverse cracks appear to cause a reduction in the high frequencies associated with the wave. Figure 28 corresponds to N=2000 cycles. The frequency spectrum of the second harmonic frequencies has disappeared. It has been shown [2] that the characteristic damage state is reached around a few thousand cycles. Therefore the presence of transverse cracking has resulted in a complete reduction in high frequencies associated with the wave. Note also that the frequency spectrum of first harmonic frequencies has become skewed and its amplitude has decreased. The skewness of the spectrum increases until about 35,000 cycles. Jamison [2] has shown that around this level of cycling the micro-delaminations that have been growing reach a fairly widespread distribution in the entire laminate. Around N=35,000 cycles the frequency spectrum becomes Gaussian again. As cycling continues, micro-delaminations enlarge gradually and the amplitude of the spectrum decreases gradually, Figs. 29 to 31. At N=95,000 cycles, Fig. 32, there is a significant drop in the amplitude of the frequency spectrum. It has been shown [2] that around 100,000 cycles, micro-delaminations tend to join together to form internal macro-delaminations. Figure 38 shows penetrant-enhanced X-ray radiographs of a $[0,90_2]_s$ graphite epoxy laminate used in this study. Figure 38a corresponds to N=70,000 cycles. Note small fuzzy areas around where the cracks intersect. These are micro-delaminations. Figure 38b corresponds to N=100,000 cycles, after a drop has been noticed both in the stiffness and the root

mean square values. Note the small areas of micro-delaminations in the interior of the specimen joined together to form macro-delaminations.

At N=140,000 cycles, Fig. 33, the amplitude of the spectra decreases further. After this the amplitude remains nearly constant, Fig. 34, with cycling reflecting the Stage II behavior of this particular laminate [2]. The root mean square values of these frequency spectra correlated well with the reduction in stiffness load cycles because of damage, Fig. 35. Note that the reduction in the root mean square values is about 60% whereas the reduction in stiffness because of damage is only about 13%. Therefore the root mean square of the frequency spectra exhibits a larger decrease than the stiffness.

For $[0,90_2]_s$ graphite epoxy laminates transverse cracks occur at 0.4% strain. When f_o, f_c, and f_p (see section 2.2.1) were plotted versus strain, there was a sudden decrease in these values at 0.4% strain, Figs. 36 and 37. This suggests that the parameters f_o, f_c, and f_p, which are ratios of various moments of the frequency spectrum could also be used to monitor damage development in composite laminates.

$[0,\pm45]_s$ Laminate

Figure 39 shows the signal and the frequency spectrum for a $[0,\pm45]_s$ graphite epoxy laminate at N=0 and P=0. The frequency spectrum for this specimen is not as well defined as for the $[0,90_2]_s$. The frequencies are spread between 100 kHz and 1 MHz. Figure 40 corresponds to N= $1/2$ and P=mean load=1345 lbs. There is no significant change in the spectrum. The strain levels are not sufficient at this load to cause matrix cracking in the ±45° plies. Figure 41 corresponds to

N=1000 cycles. There is a small decrease in the amplitude of the spectrum over the entire frequency range. Figures 42 through 45 correspond to N=21,000 cycles, 35,000 cycles, 45,000 cycles and 95,000 cycles. The amplitude of the spectrum gradually decreased with increasing cycles. It has been reported [2] that the damage modes in these laminates are restricted to matrix cracking in the ±45° plies and longitudinal splitting in the 0° plies. There is no significant delamination. This is believed to be one of the reasons why a sudden drop in the $(M_0)^{1/2}$ and stiffness values with cycling as in the case of $[0,90_2]_s$ laminates does not occur. Figure 46 shows that the root mean square values of the spectra correlated quite well with the stiffness reduction with cycles. Note that the $(M_0)^{1/2}$ exhibits a larger decrease than stiffness.

$[0,90,\pm45]_s$ Laminate

Figure 47 shows the signal and its frequency spectrum at N=0 and P=0. The spectrum appears to be somewhat between that of a $[0,90_2]_s$ and a $[0,\pm45]_s$ spectra. Figure 48 corresponds to N=$\frac{1}{2}$ and P=mean load=1254 lbs. There is no significant change in the spectrum. Figure 49 corresponds to N=20,000 cycles. There is a small decrease in the amplitude of the frequency spectrum. At N=30,000 cycles, Fig. 50, the amplitude drops by a considerable amount. It has been reported [2] that around 25,000 cycles, delaminations grow slowly from the free edges into the specimen. Visual confirmation of edge delamination was made at N=50,000 cycles, Fig. 51, for the specimen being tested. Figure 52 shows that the root mean square values of the spectra correlate quite

well with reduction in stiffness with load cycles, because of damage. Note that the $(M_o)^{1/2}$ exhibits a larger decrease than stiffness.

Therefore, in all three laminate types tested, there was an excellent correlation between the root mean square values, stiffness, and damage development in controlled cyclic loading. In all cases, the $(M_o)^{1/2}$ exhibited larger decreases than the stiffness. A computer program to calculate $(M_o)^{1/2}$, f_p, f_c, and f_o was developed to save computation time. The signal received by the receiving transducer, after appropriate signal conditioning, is sent through a transient wave form recorder and then to the computer. The computer program calculates $(M_o)^{1/2}$, f_p, f_c, and f_o for the spectrum of each signal (see Fig. 53).

3.3 Usefulness of the SWF as an NDT Technique

From the results and discussion reported thus far, it is clear that there is indeed a correlation between $(M_o)^{1/2}$, stiffness, and damage in thin composite laminates. The SWF technique is particularly useful because it yields a single parameter, such as $(M_o)^{1/2}$, to characterize the damage, and the effects of various forms of damage between the transducers in integrated, very much like the stiffness. From an engineering standpoint this feature has tremendous significance. The parameter so obtained could be used in a damage parameter-stiffness-life model [26] to predict the mechanical response of the material because of the presence of damage.

Advantages of the SWF Technique

- This technique yields quantitative parameters, like $(M_0)^{1/2}$, which can be correlated with the stiffness of composite materials.
- $(M_0)^{1/2}$ exhibited larger decreases than stiffness for cyclically loaded composites.
- It requires access to only one side of the structure, which is of great practical importance.
- It has the potential to be used as an integral NDT system with a structure to monitor damage development.

Limitations of the SWF Technique

- This technique cannot provide a precise geometric description of damage in the material.
- The strength of the signal changes with the distance between transducers.
- A unique relationship between strength and the parameter obtained by SWF is not possible.

4. CONCLUSIONS

The conclusions arrived at from this study are listed below.

- The SWF has excellents potential as an NDT technique for thin composite laminates.
- The results of other NDT techniques such as moiré interferometry and ultrasonic C-scan support the SWF results.
- SWF is the highest along the fiber direction and the lowest across the fibers.
- SWF appeared to interrogate the top 3 to 4 plies of the laminate for the test conditions used in this study.
- An alternative "SWF" method, which makes use of the root mean square values of the frequency spectrum of the received signal was developed.
- This alternate method does not need a threshold level and hence is more practical.
- The root mean square of the frequency spectrum correlated with the reduction in the laminate stiffness during cyclic loading for the three stacking sequences of the laminates were tested: $[0,90_2]_s$, $[0,\pm45]_s$, and $[0,90,\pm45]_s$.
- The root mean square values exhibited larger decreases than stiffness, during cyclic loading of composite laminates.
- The root mean square values have potential to provide insight into the nature of damage development.

Recommendations for Future Work

- Perform basic experiments to understand the nature of wave propagation in composite laminates.
- Perform systematic experiments to correlate the exact nature of damage (as seen by X-ray radiography, edge replication, etc.) with the various moments of the frequency spectrum.

Table I

Specimen $[0,90_2]_s$ Gr/Ep

N	E	E/E_o	M	M/M_o
0	$7.34 \times 10^3 (=E_o)$	1.00	$493.25 \times 10^{-5} (=M_o)$	1.00
1/2	7.12×10^3	0.97	428.75×10^{-5}	0.93
2,000	6.97×10^3	0.95	307.84×10^{-5}	0.79
6,000	6.90×10^3	0.94	262.85×10^{-5}	0.73
16,000	6.83×10^3	0.93	248.65×10^{-5}	0.71
30,000	6.83×10^3	0.93	202.03×10^{-5}	0.64
95,000	6.53×10^3	0.89	195.77×10^{-5}	0.63
140,000	6.46×10^3	0.88	82.91×10^{-5}	0.41
270,000	6.38×10^3	0.87	67.52×10^{-5}	0.37

All measurements made with cycling stopped and P=mean load=1248 lbs.
Units for E are ksi; units for M are volts/sec.

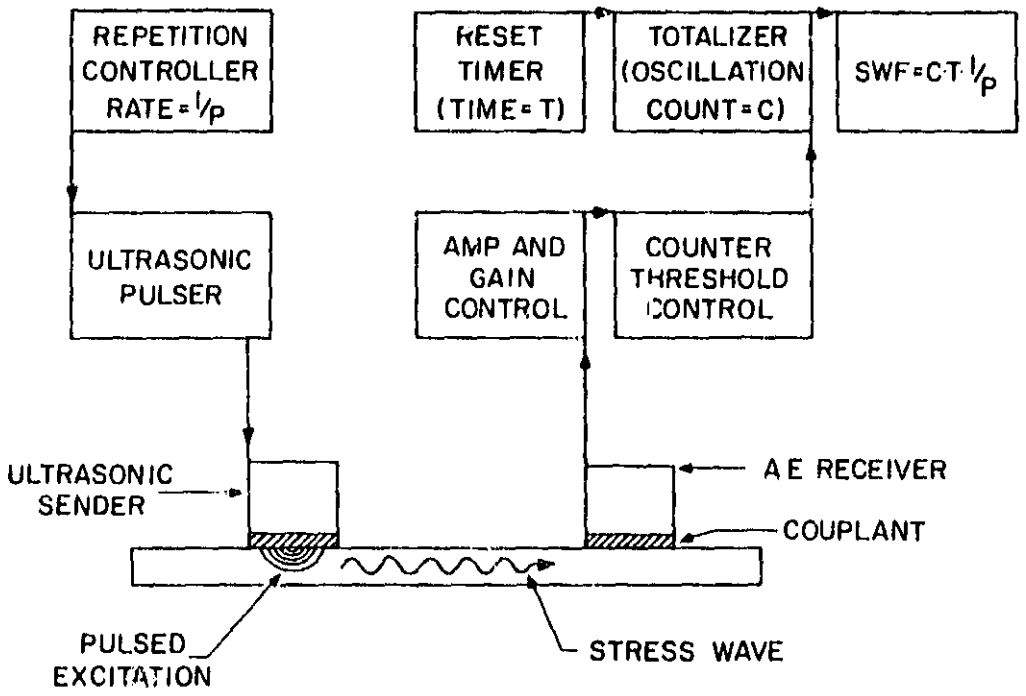

Fig. 1. Schematic of the SWF set-up.

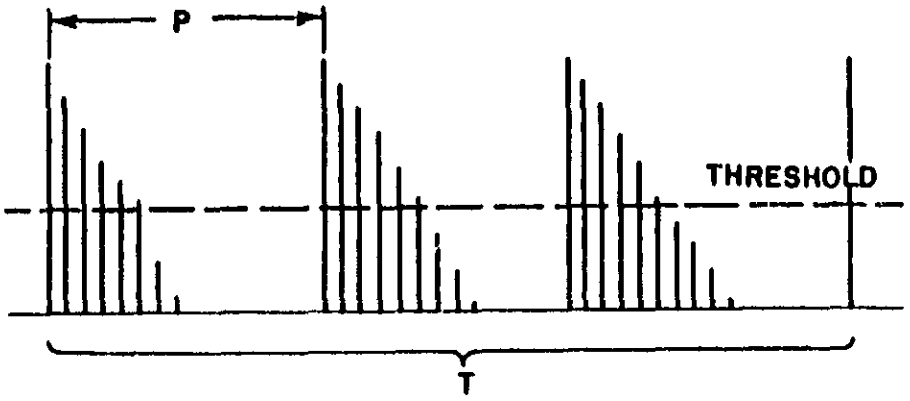

Fig. 2. Definition of SWF.

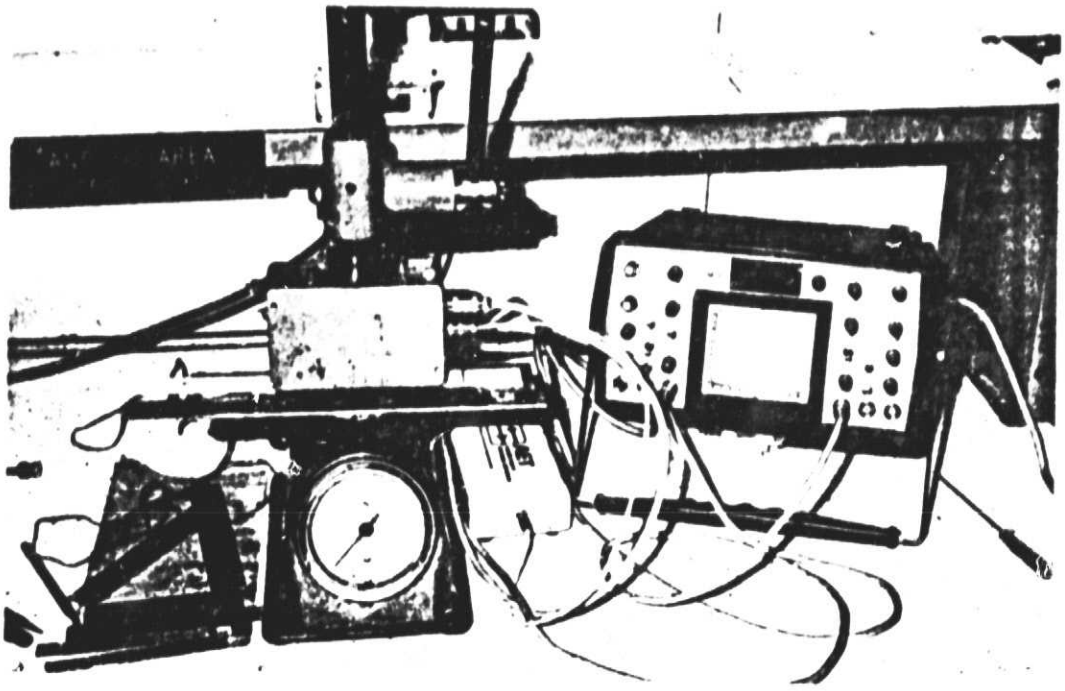

Fig. 3. AET model 206 AU and the spring loading instrument.

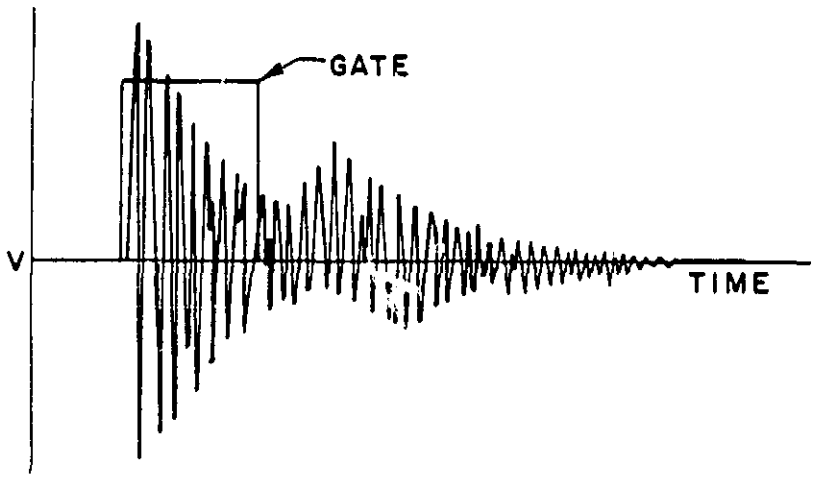

Fig. 4. Signal-gate-threshold interrelationship.

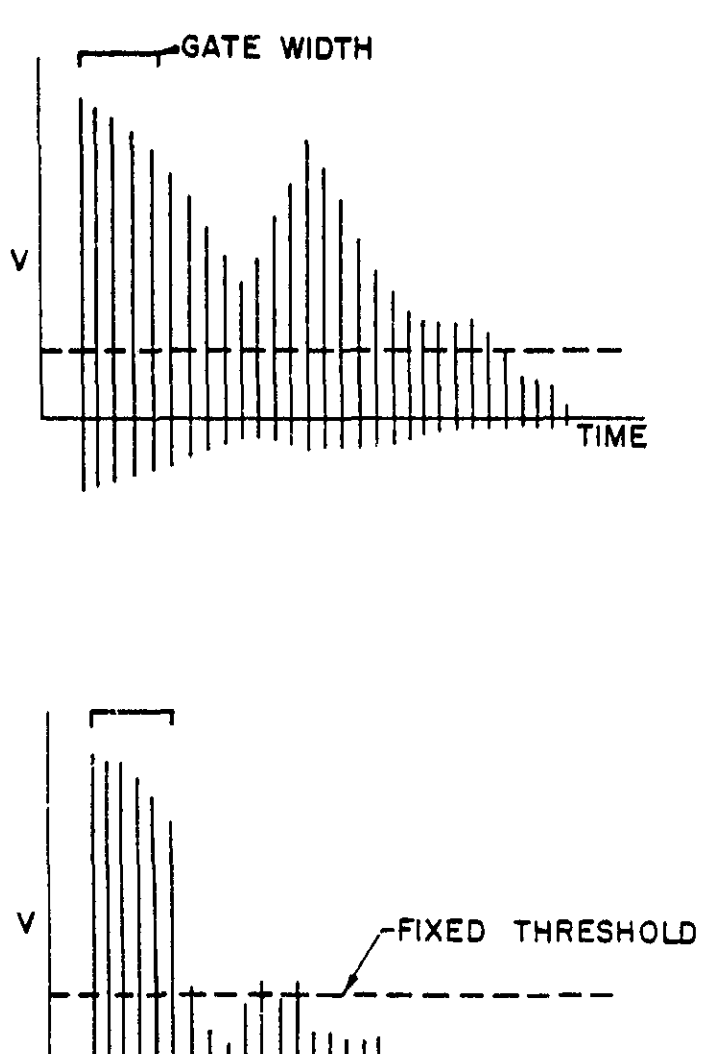

Fig. 5. Narrow gate width at two different threshold levels yielding approximately the same number of counts for two substantially different signals.

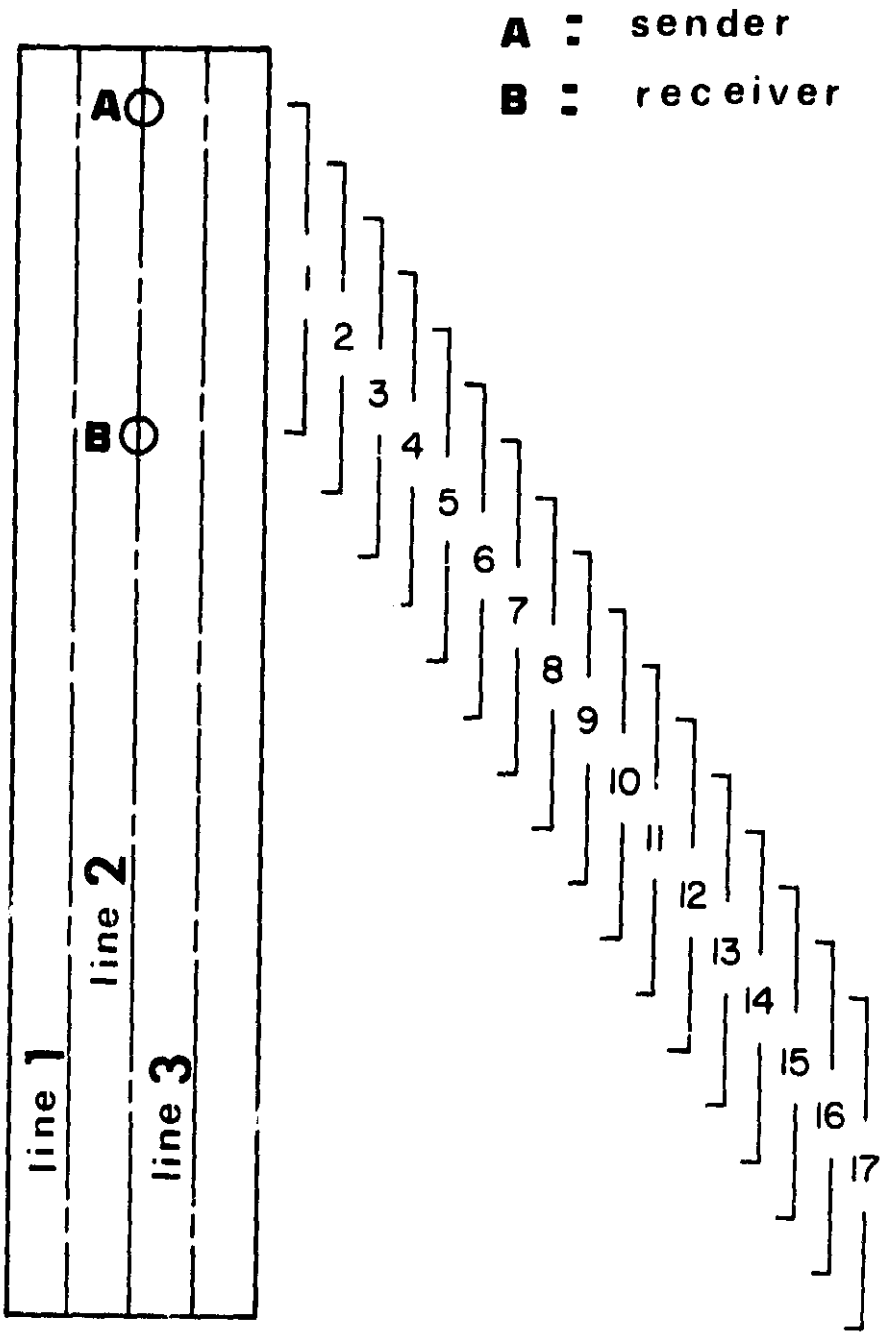

Fig. 6. Schematic showing the location of the SWF measurements made on the specimen.

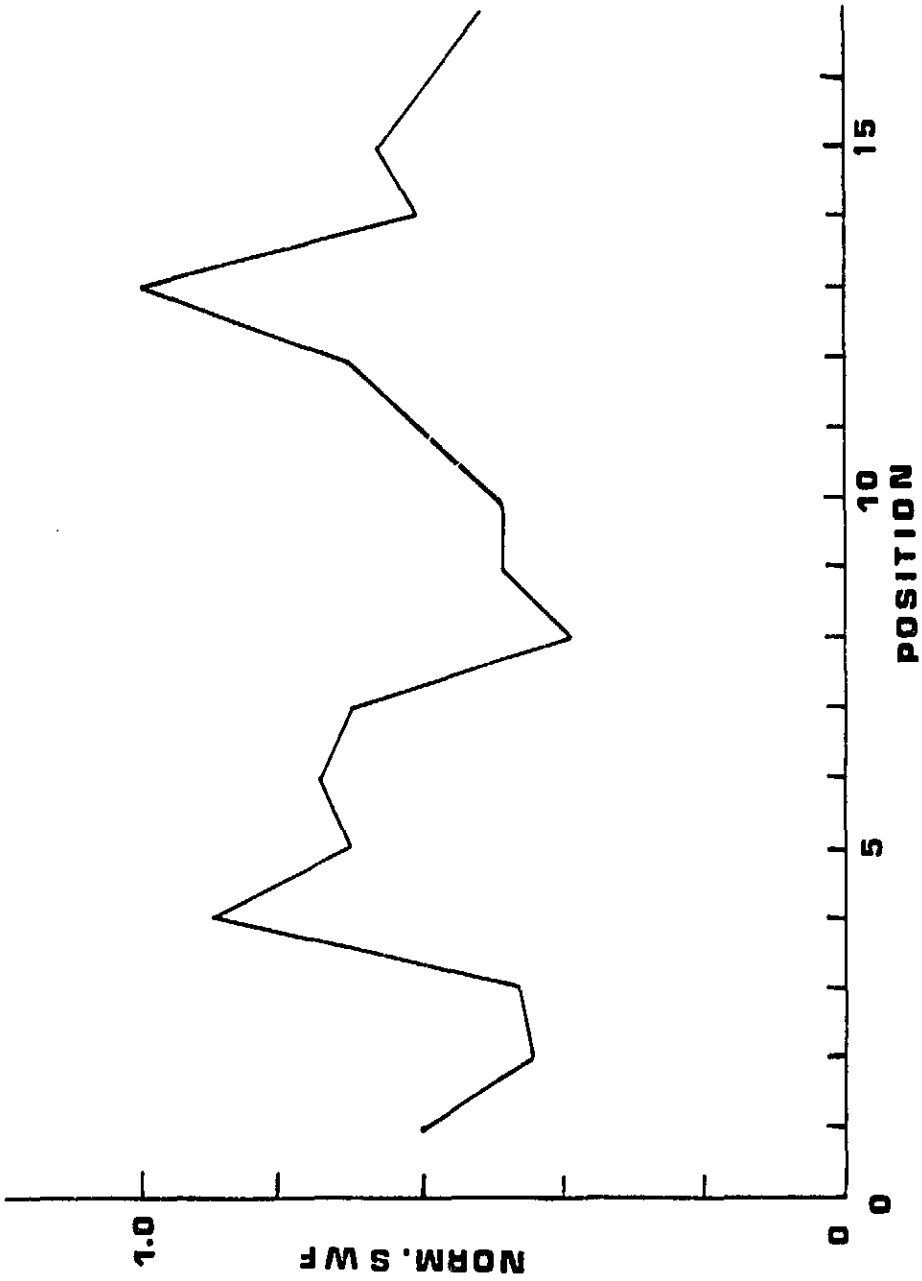

Fig. 7. Plot of the normalized SWF vs. position on specimen. Low values of SWF indicate weak regions and vice versa.

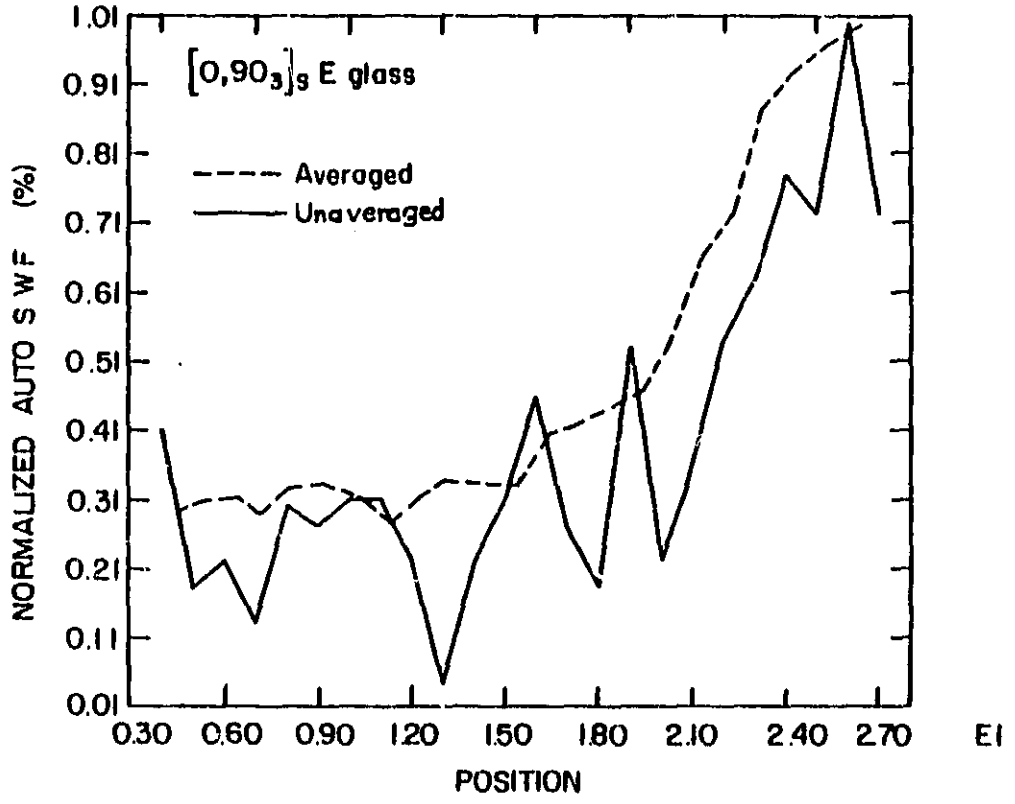

Fig. 8. Comparison of the SWF data with and without averaging.

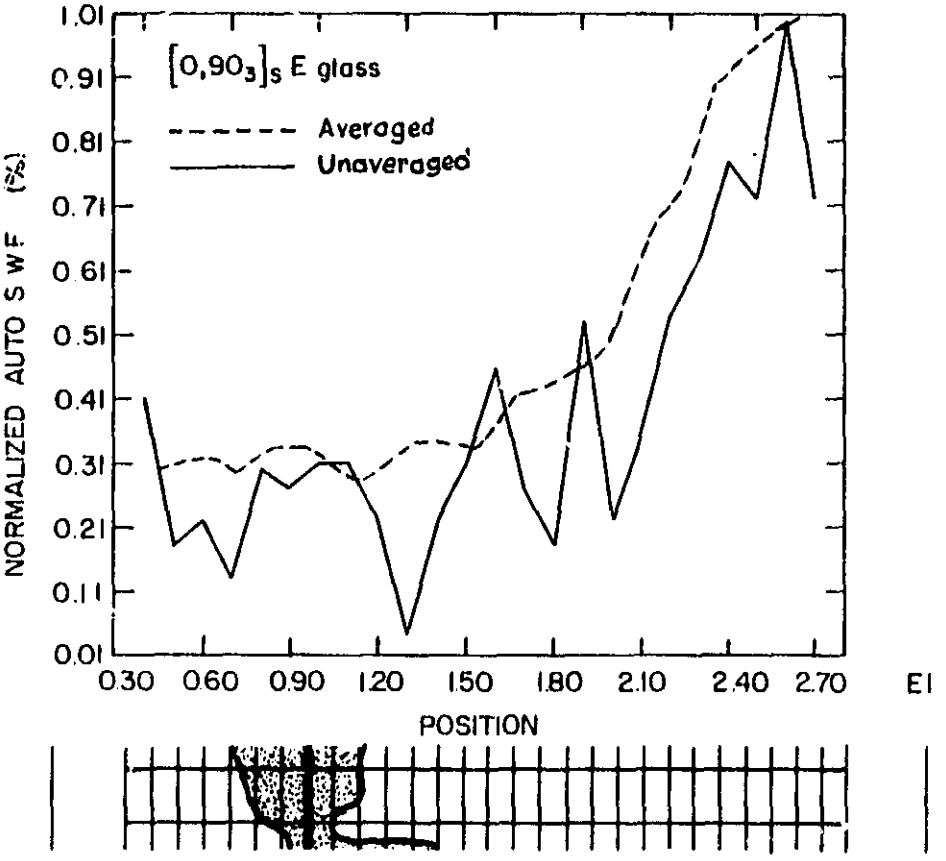

Fig. 9. Correlation of SWF with specimen failure location.

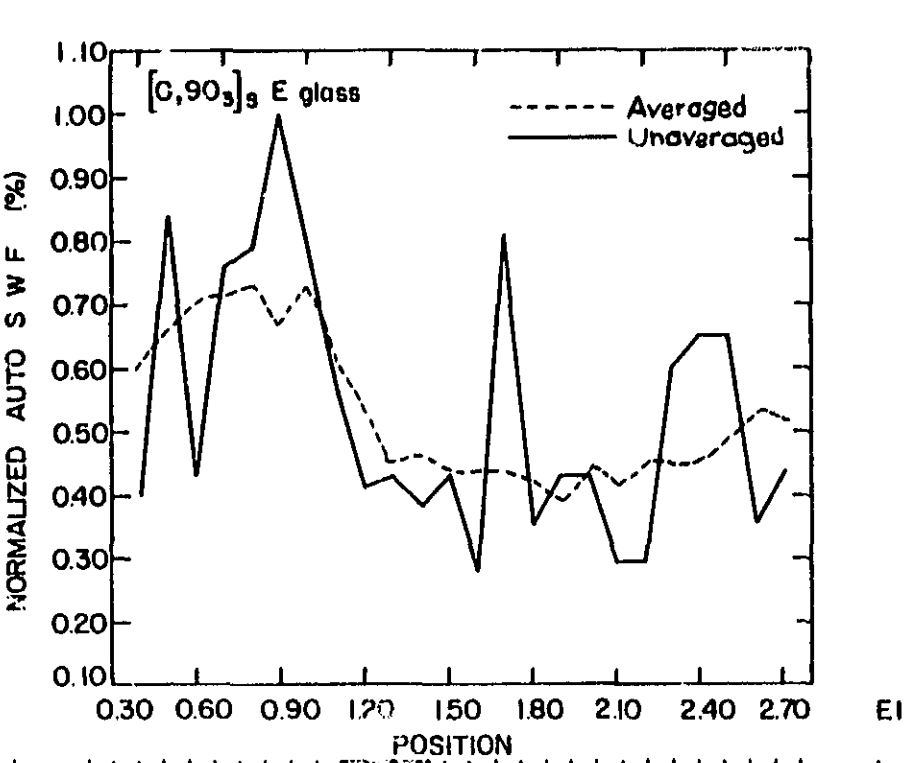

Fig. 10. Correlation of SWF with specimen failure location.

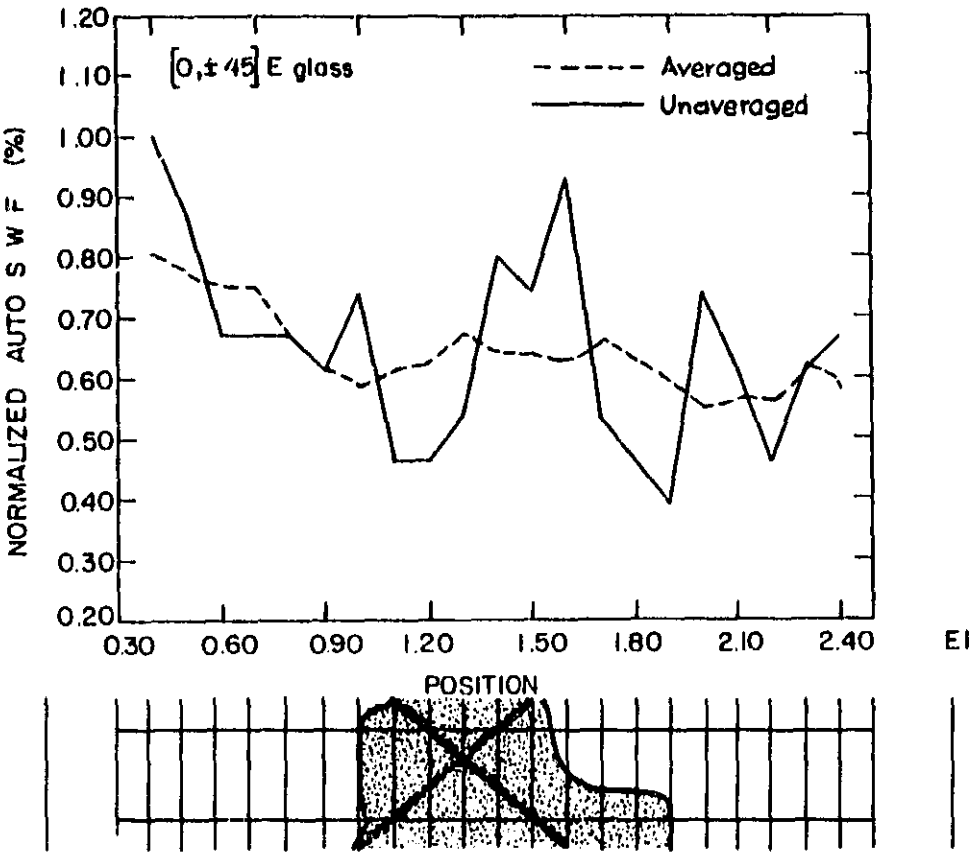

Fig. 11. Correlation of SWF with specimen failure location.

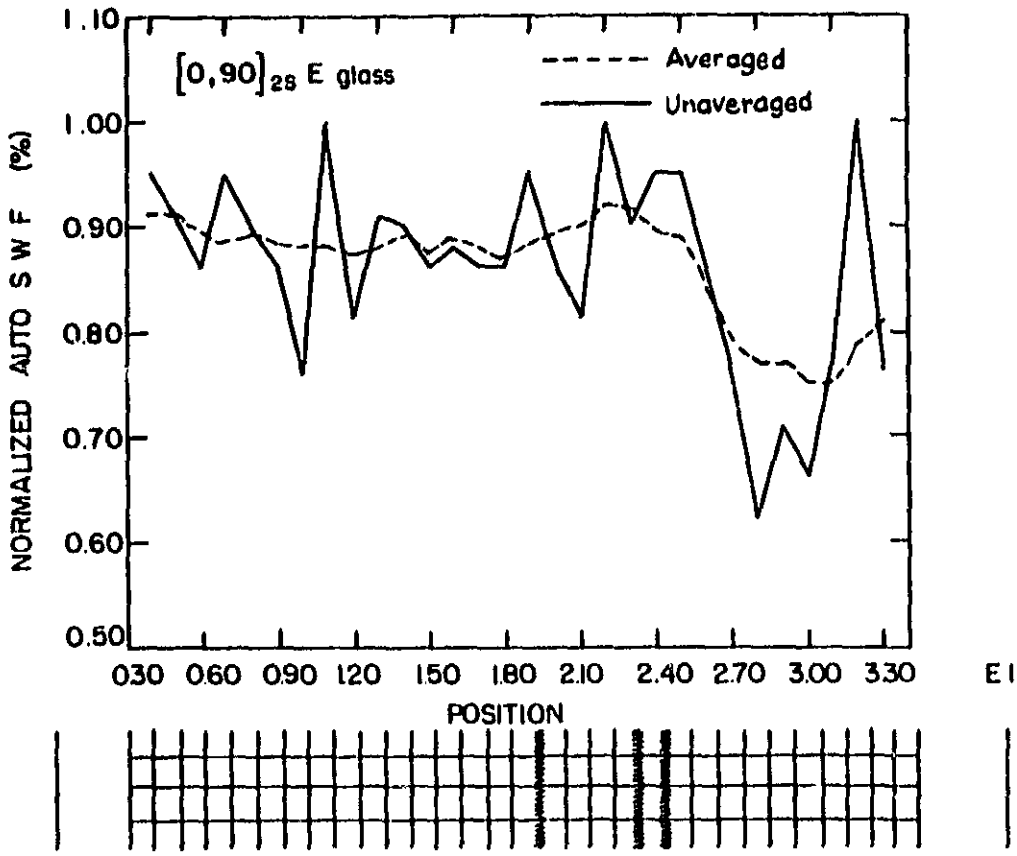

Fig. 12. Correlation of SWF with specimen failure location.

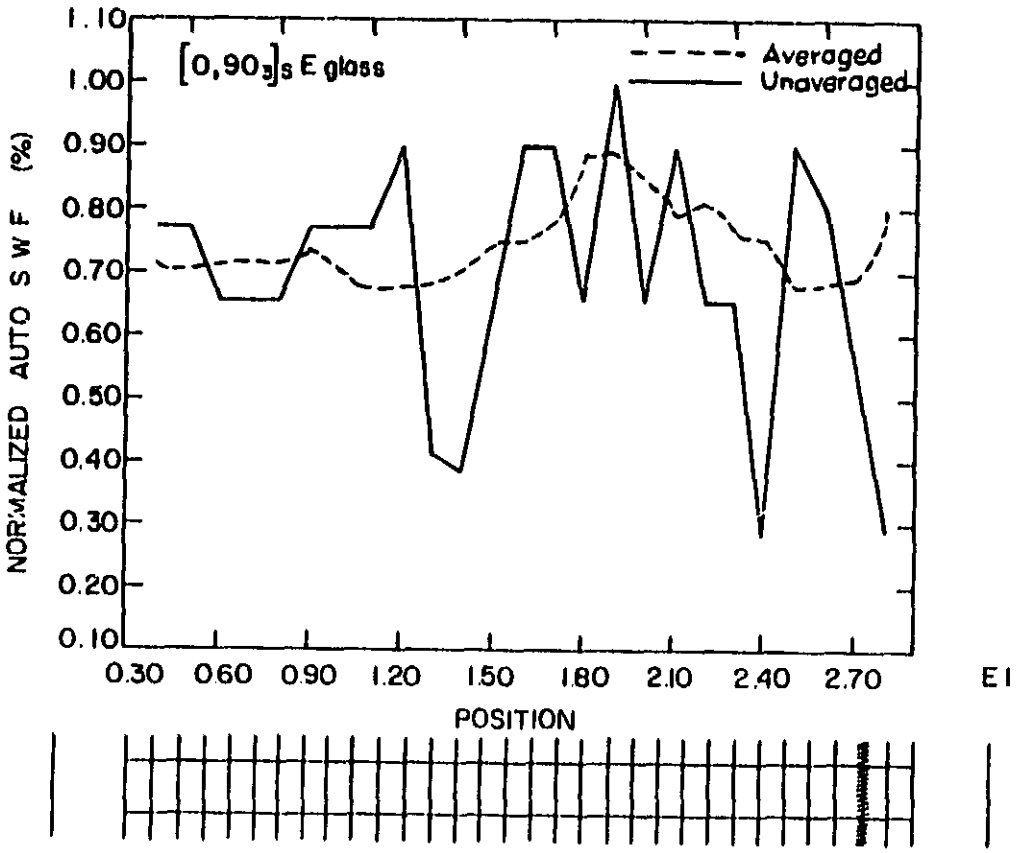

Fig. 13. Correlation of SWF with specimen failure location.

Fig. 14. Ultrasonic C-scan of a virgin $[0,90_3]_s$ E-glass epoxy specimen. Note indication of flaws at the top end, center, and the bottom end of the specimen.

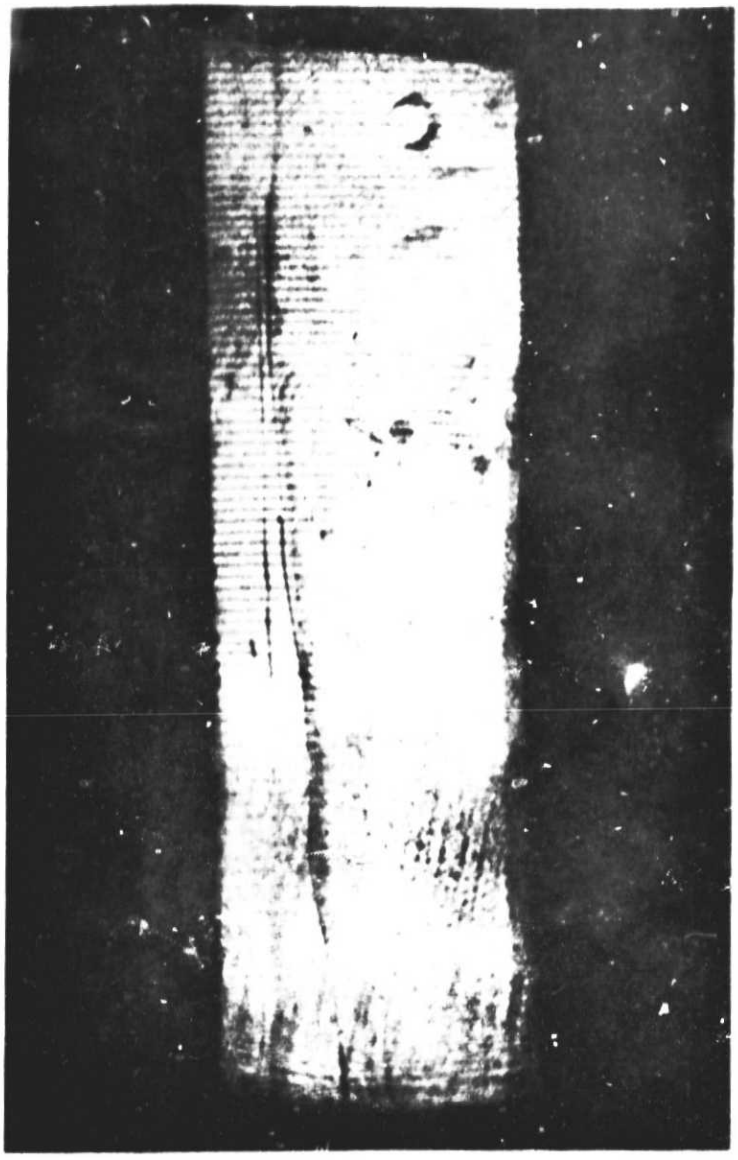

Fig. 15. Moiré fringe pattern (u displacement field) of a $[0,90_3]_s$ E-glass epoxy specimen at 500 $\mu\varepsilon$. Note the uniform displacement field along the length of the specimen.

Fig. 16. Moiré fringe pattern (u displacement field) at a $[0,90_3]_s$ E-glass epoxy specimen at 2000 με. Note that the top end, center, and the bottom end of the specimens have higher displacements compared to other regions.

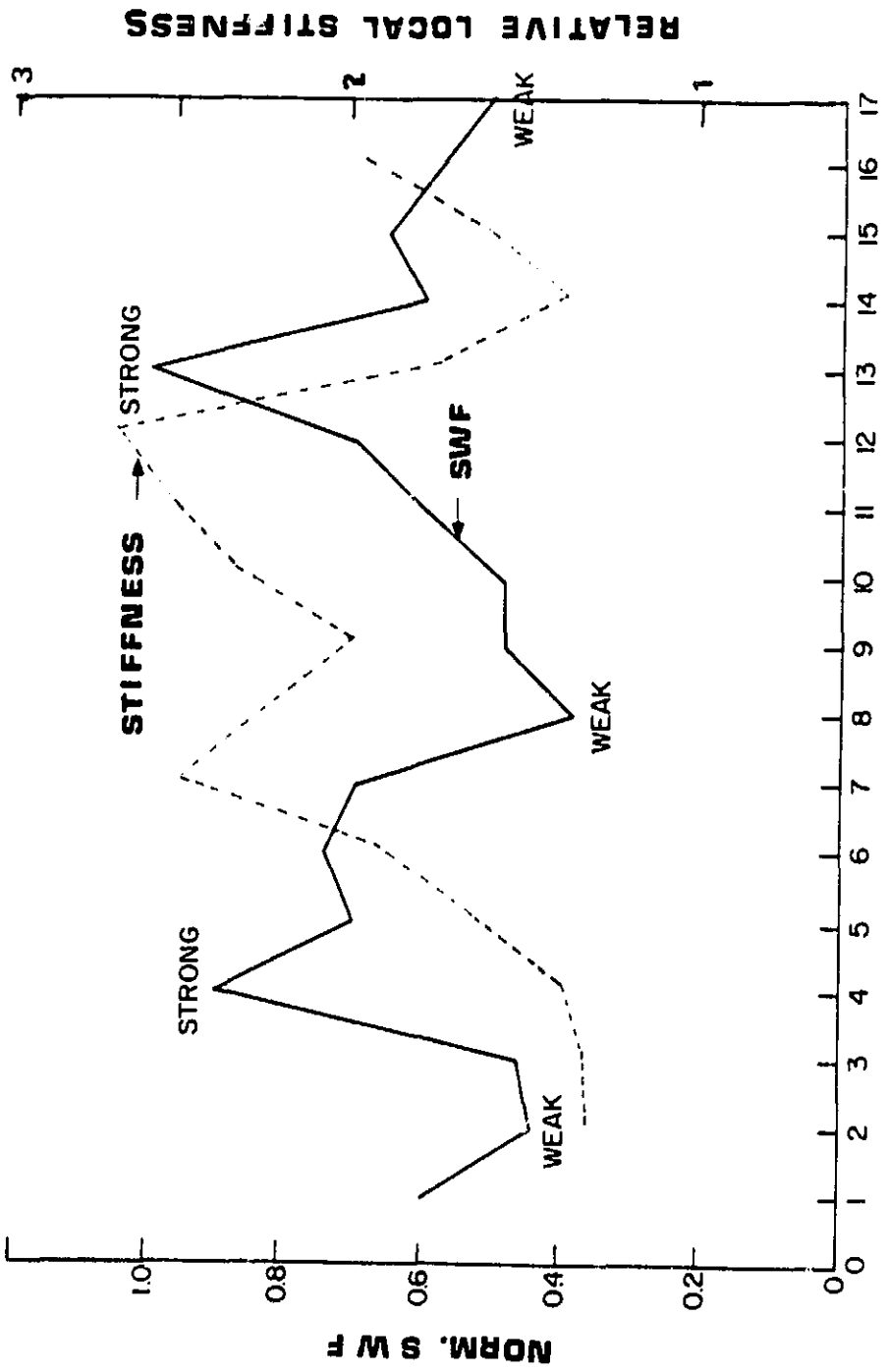

Fig. 17. Plot comparing normalized SWF and local stiffnesses vs. position on specimen.

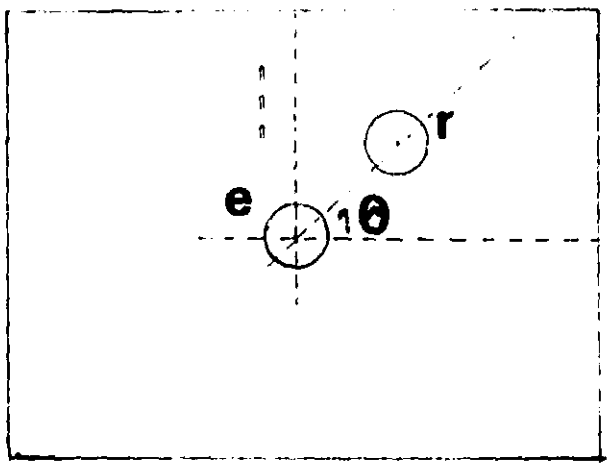

Fig. 18. Schematic of the set-up to evaluate the effect of fiber orientation on the SWF, e = sender, r = receiver.

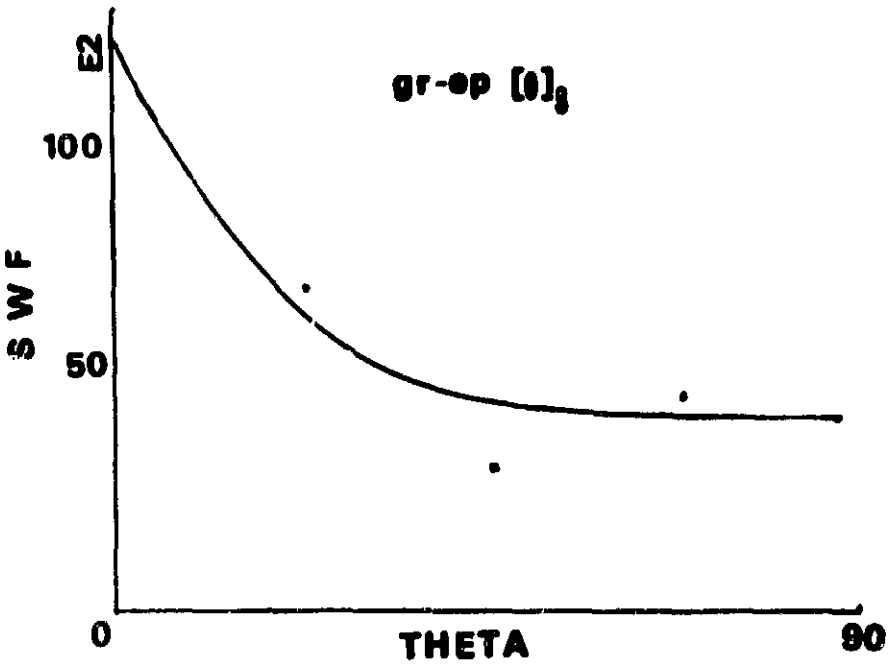

Fig. 19. Variation of the SWF with fiber orientation.

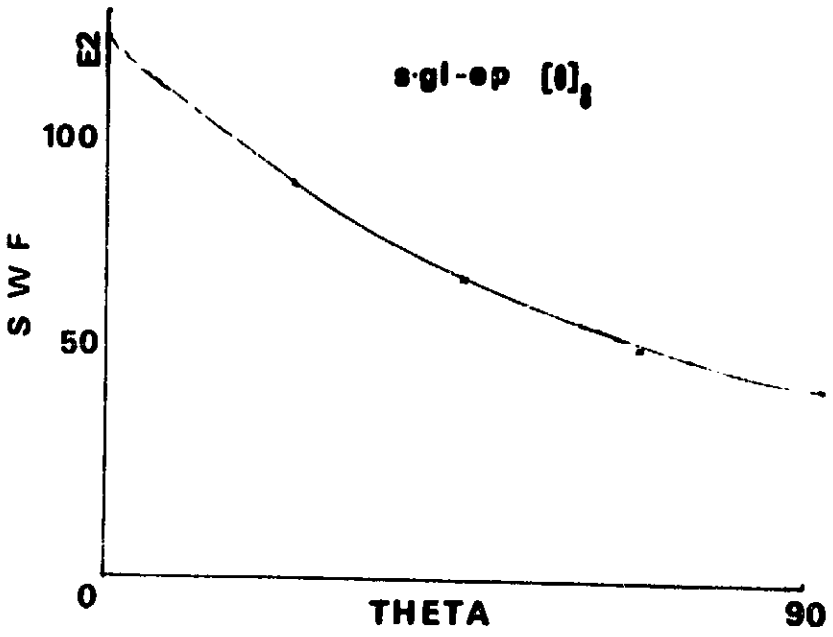

Fig. 20. Variation of the SWF with fiber orientation.

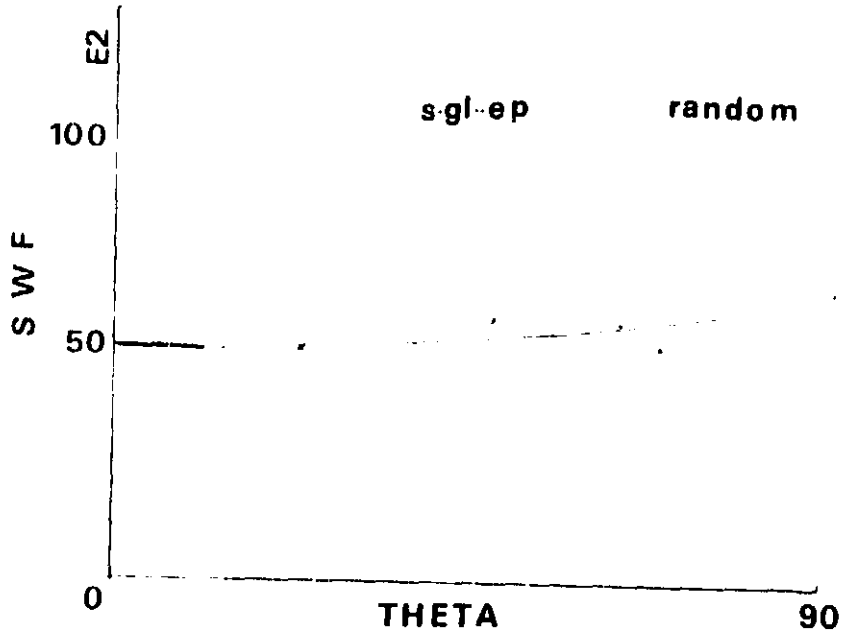

Fig. 21. Variation of the SWF in an arbitrarily chosen 0° to 90° quadrant of a random fiber S-glass epoxy panel.

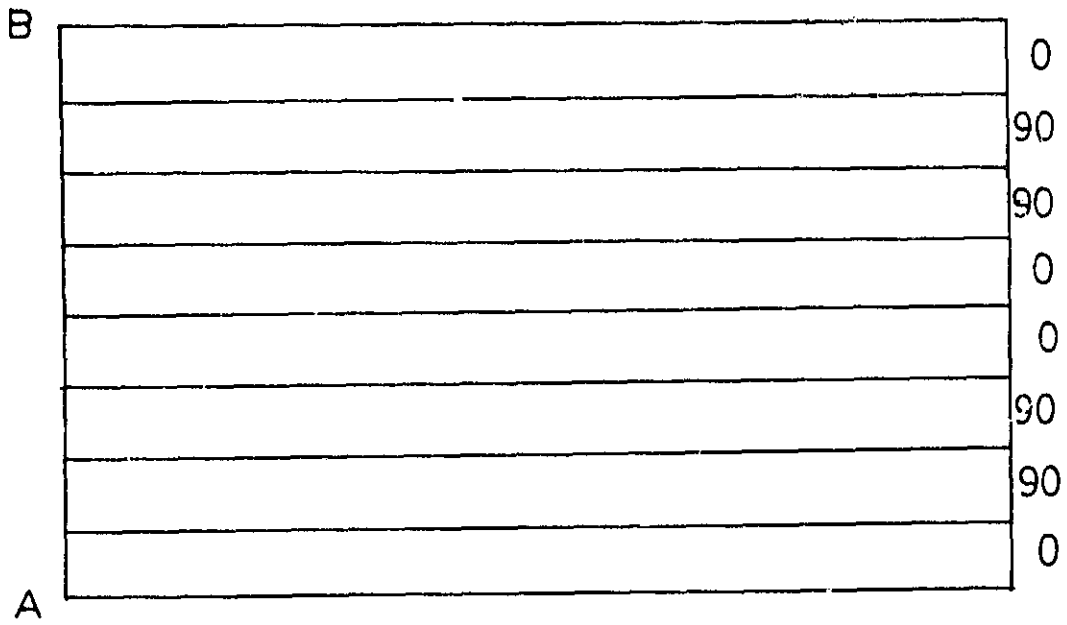

Fig. 22a. Schematic of an edge replica of an undamaged $[0,90_2,0]_s$ graphite epoxy specimen.

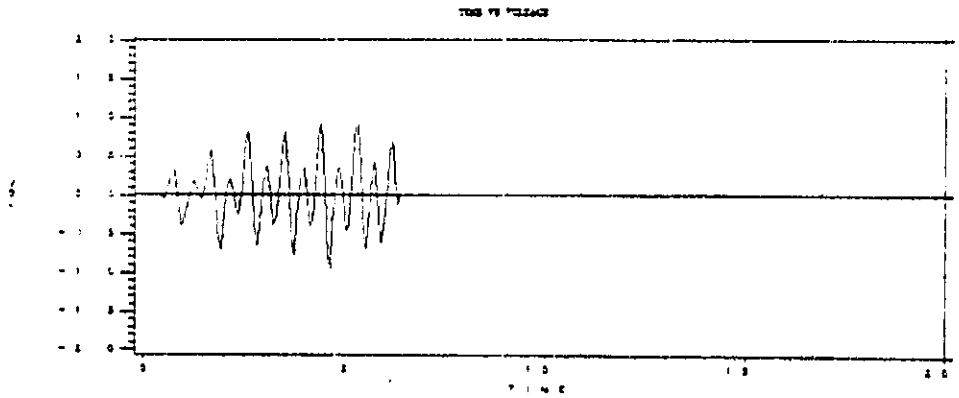

Fig. 22b. Acousto-ultrasonic signal on side A of an undamaged $[0,90_2,0]_s$ specimen.

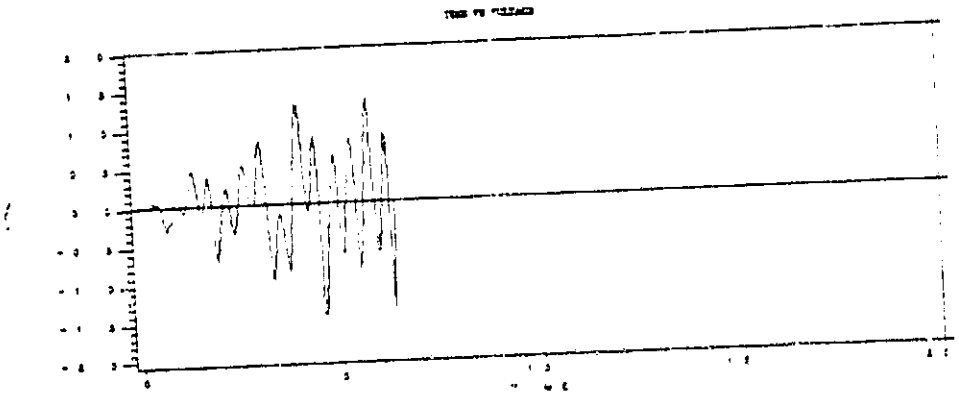

Fig. 22c. Acousto-ultrasonic signal on side B of an undamaged $[0,90_2,0]_s$ specimen.

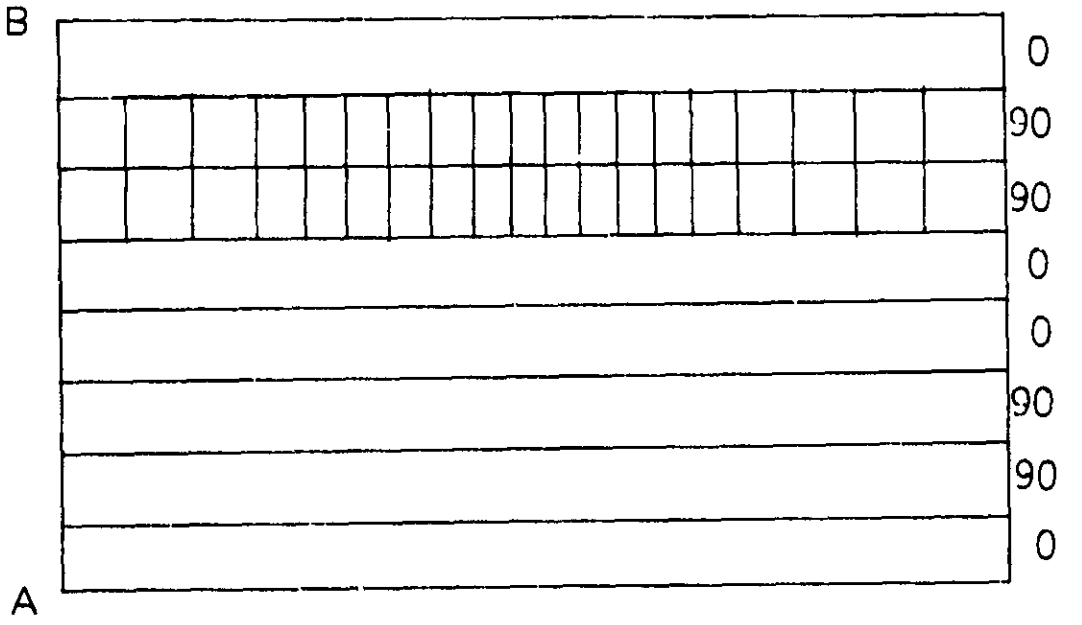

Fig. 23a. Schematic of an edge replica of a $[0,90_2,0]_s$ graphite epoxy specimen that has been bent to introduce matrix cracks in the 90° plies towards side B.

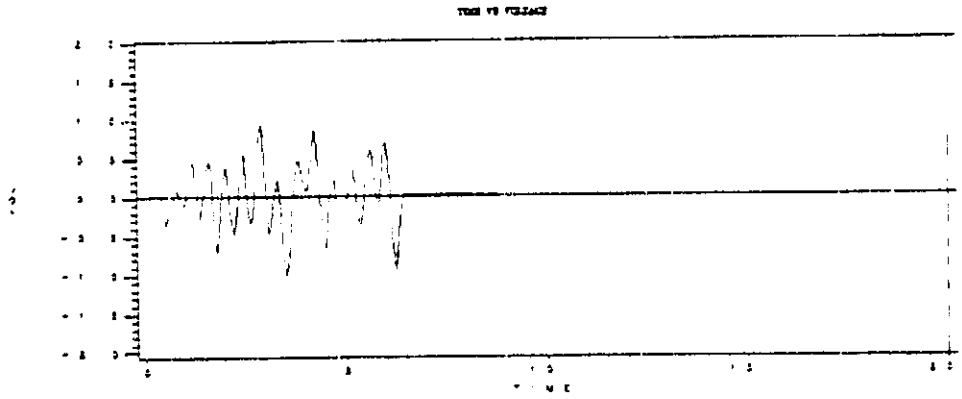

Fig. 23b. Acousto-ultrasonic signal on side A of a damaged $[0,90_2,0)_s$ specimen.

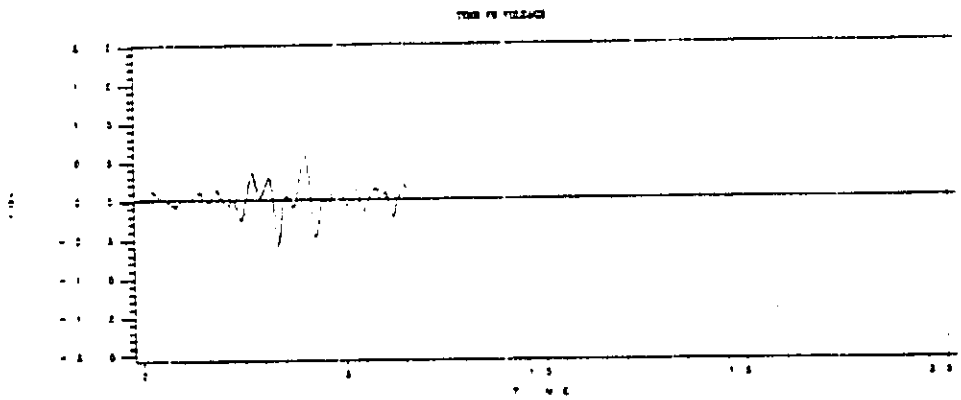

Fig. 23c. Acousto-ultrasonic signal on side B of a damaged $[0,90_2,0]_s$ specimen.

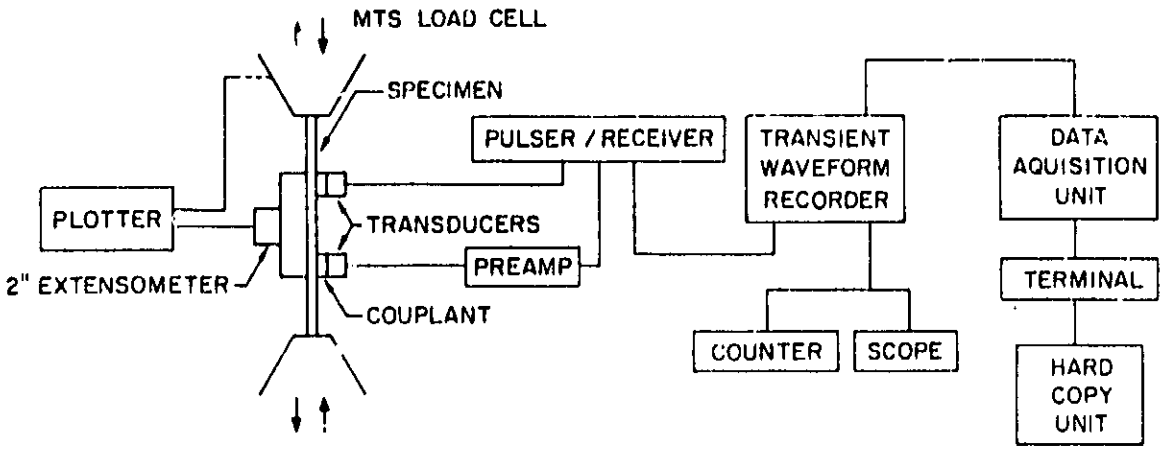

Fig. 24. Schematic of the experimental set-up to calculate the Fourier Transform of the signal.

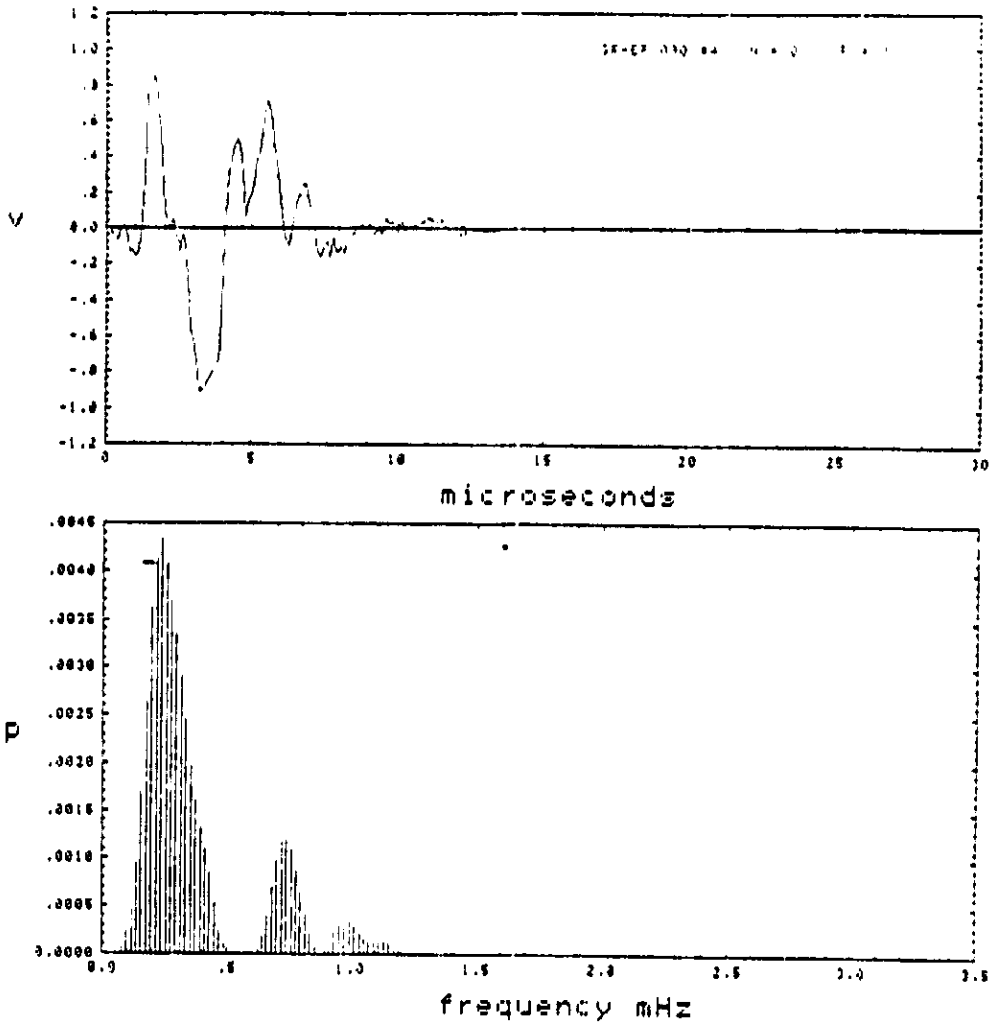

Fig. 25. A typical signal and its frequency spectrum for an undamaged $[0,90_2]_s$ graphite epoxy specimen.

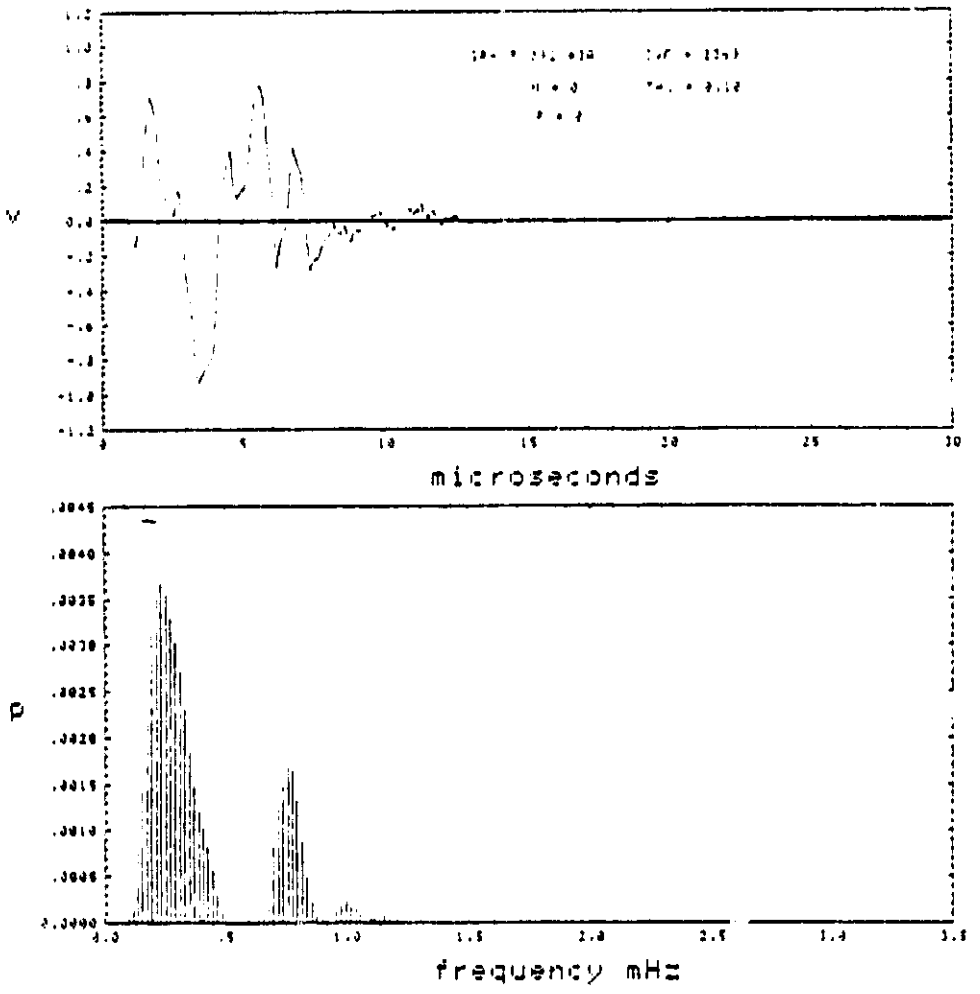

Fig. 26. The signal and its spectrum at N=0, ^{o}=0 for a $[0,90_2]_s$ graphite epoxy specimen.

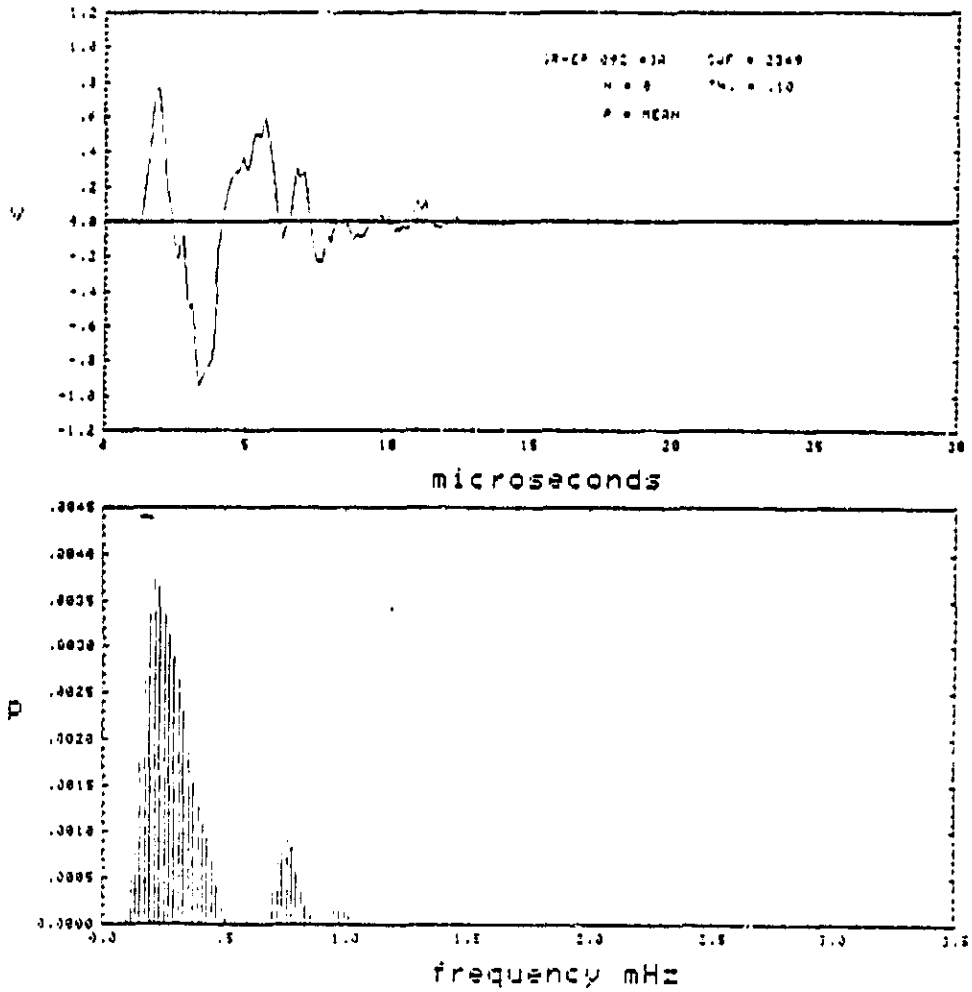

Fig. 27. The signal and its spectrum at N=½ P=1248 lbs for a $[0,90_2]_s$ graphite epoxy specimen.

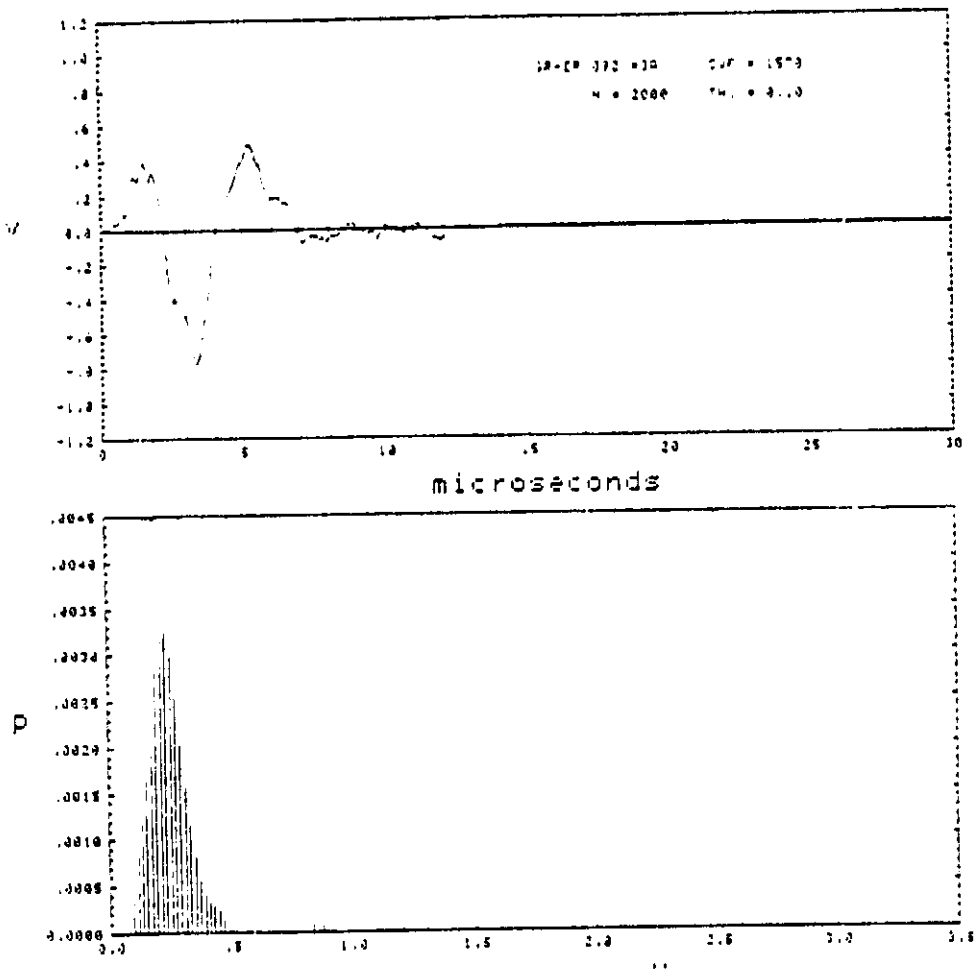

Fig. 28. The signal and its spectrum at N=2,000, P=1248 lbs for a $[0,90_2]_s$ graphite epoxy specimen.

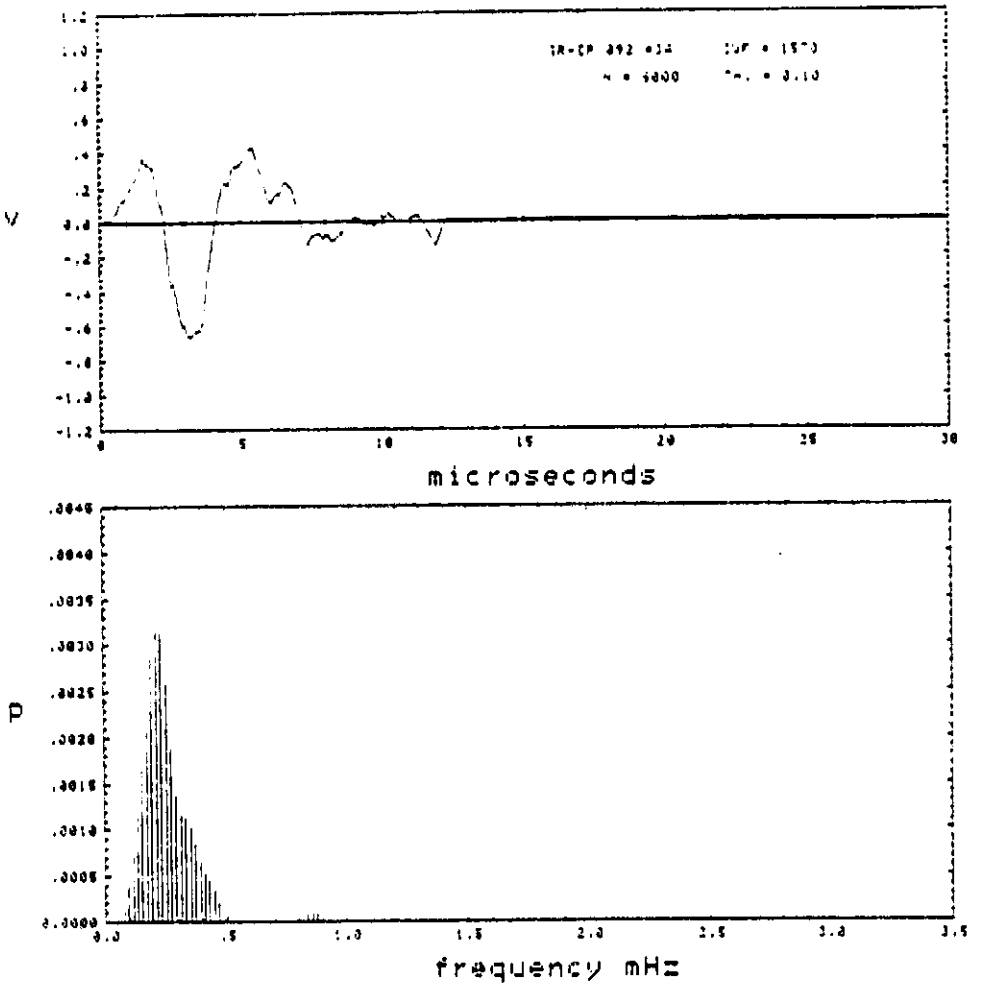

Fig. 29. The signal and its spectrum at N=6,000, P=1248 lbs for a $[0,90_2]_s$ graphite epoxy specimen.

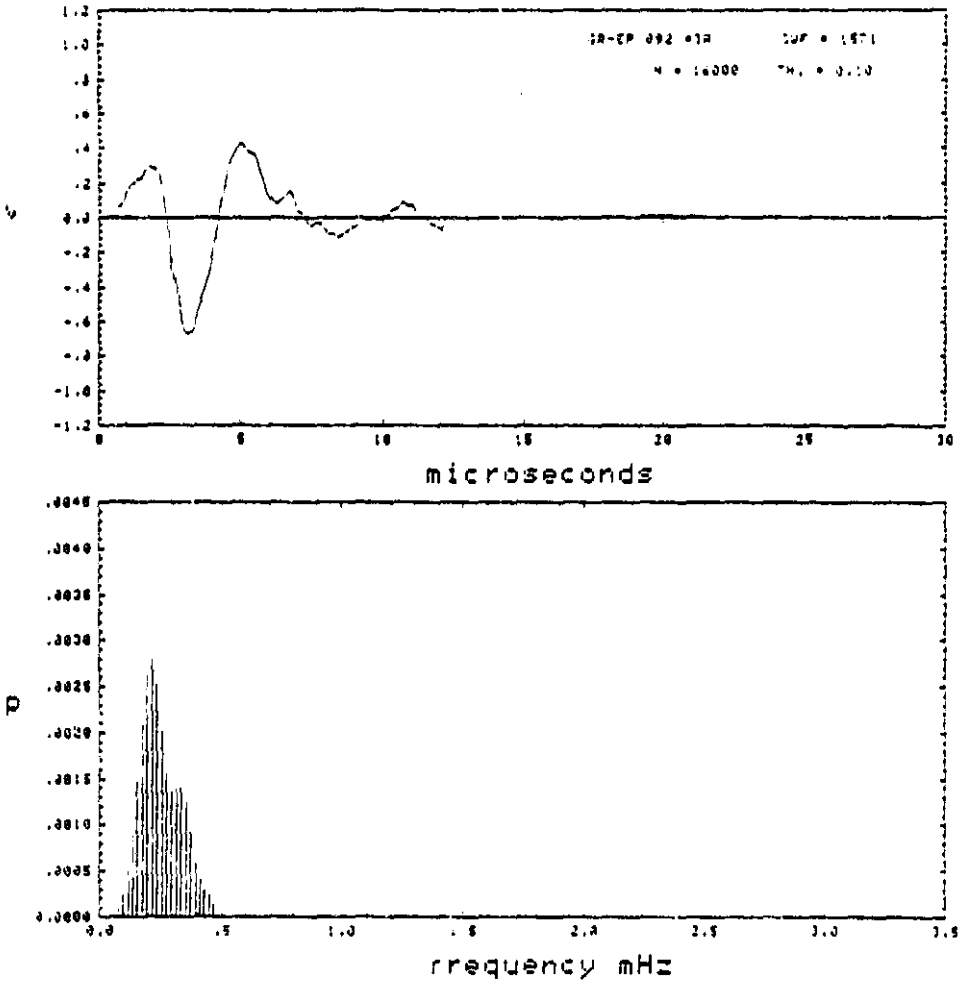

Fig. 30. The signal and its spectrum at N=16,000, P=1248 lbs for a $[0,90_2]_s$ graphite epoxy specimen.

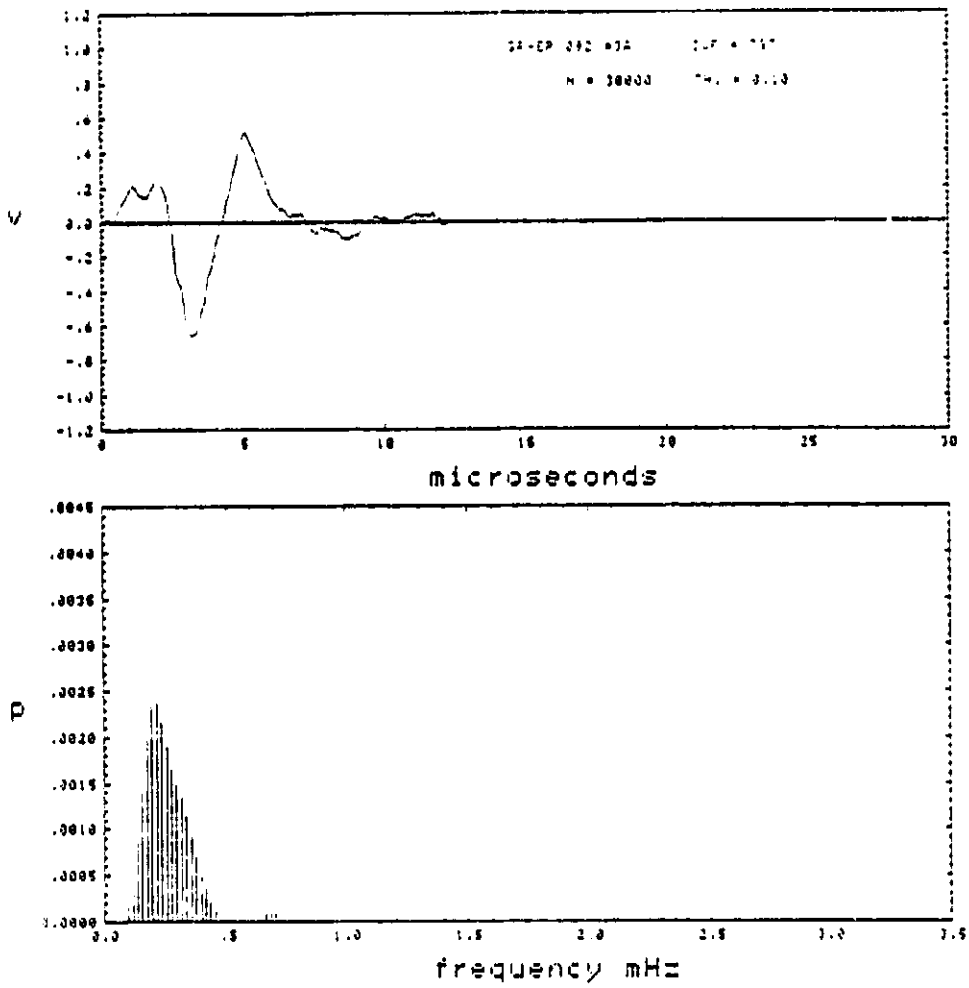

Fig. 31. The signal and its spectrum at N=30,000, P=1248 lbs for a $[0,90_2]_s$ graphite epoxy specimen.

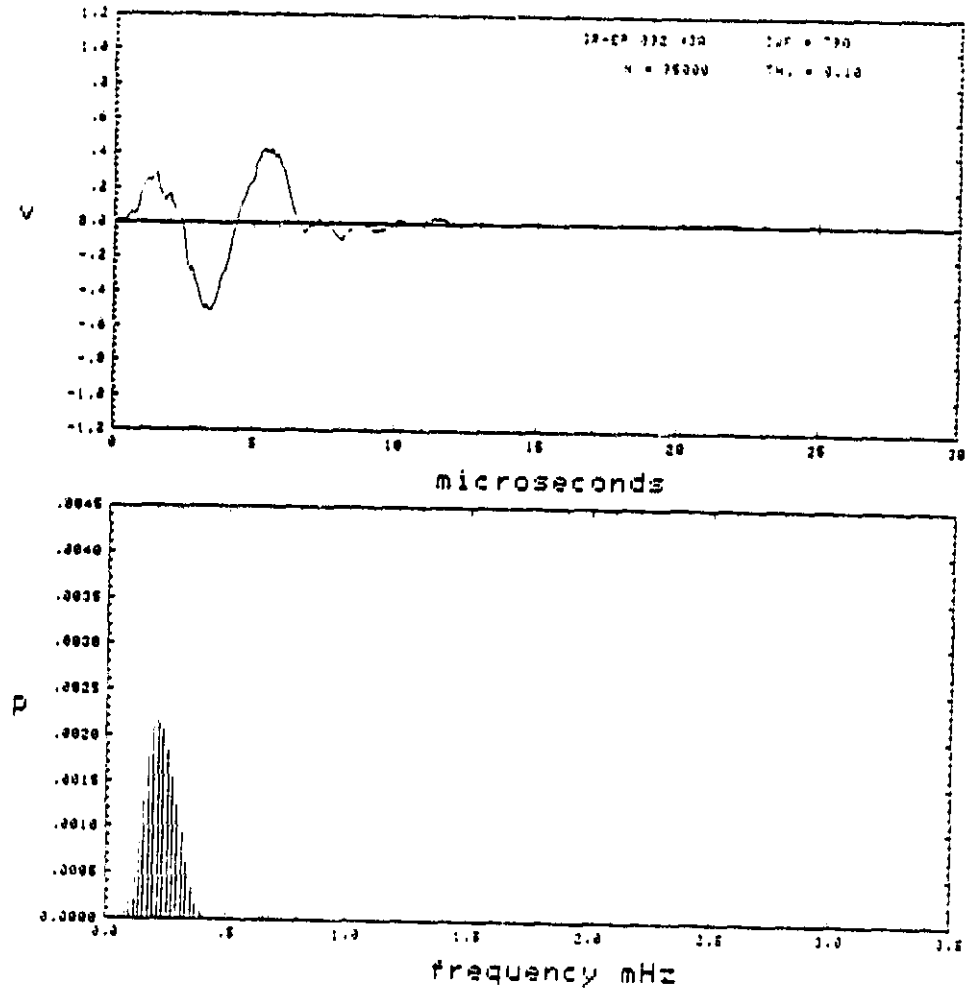

Fig. 32. The signal and its spectrum at N=95,000, P=1248 lbs for a $[0,90_2]_s$ graphite epoxy specimen.

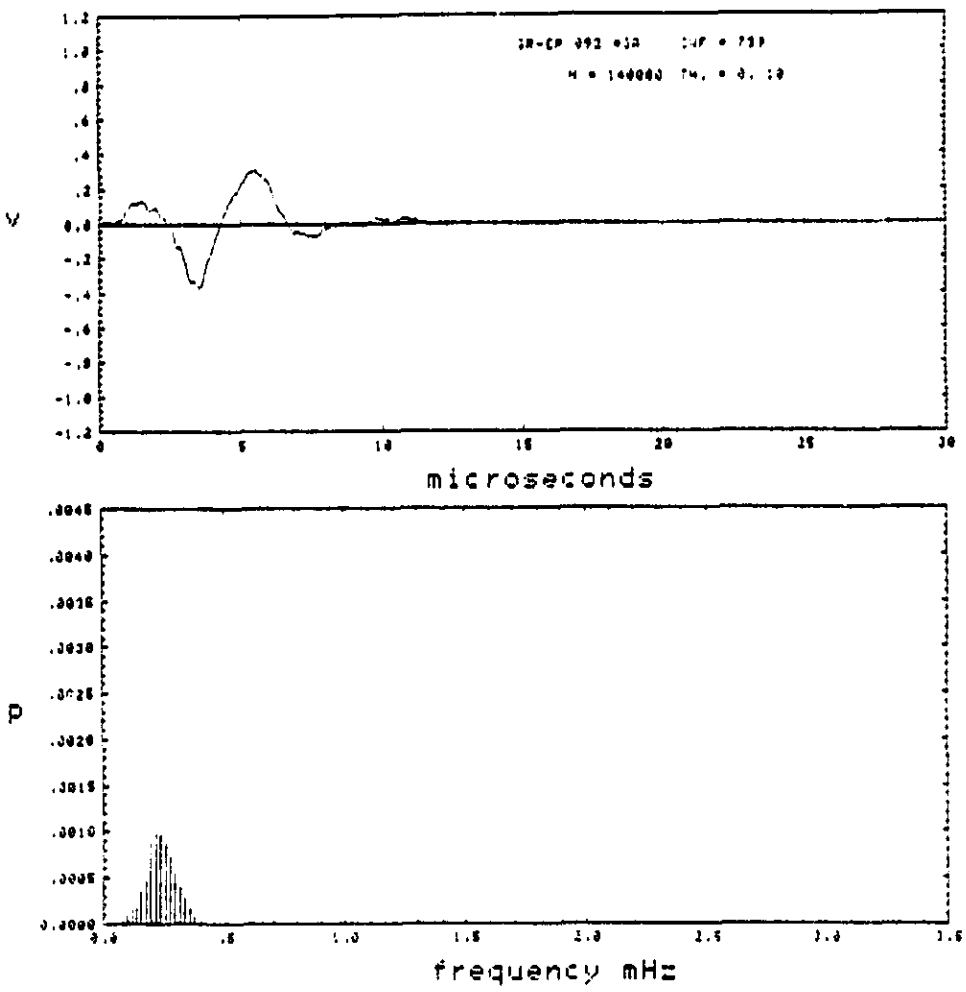

Fig. 33. The signal and its spectrum at N=140,000, P=1248 lbs for a $[0,90_2]_s$ graphite epoxy specimen.

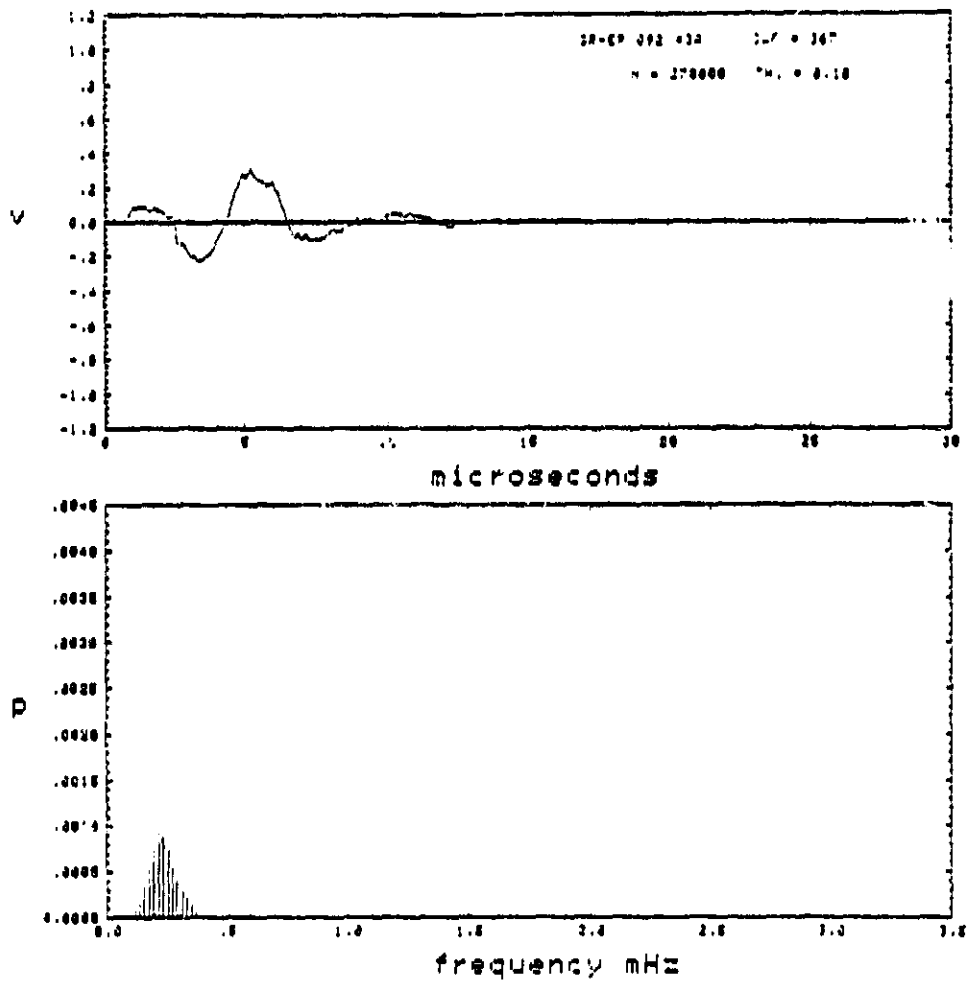

Fig. 34. The signal and its spectrum at N=270,000, P=1248 lbs for a $[0,90_2]_s$ graphite epoxy specimen.

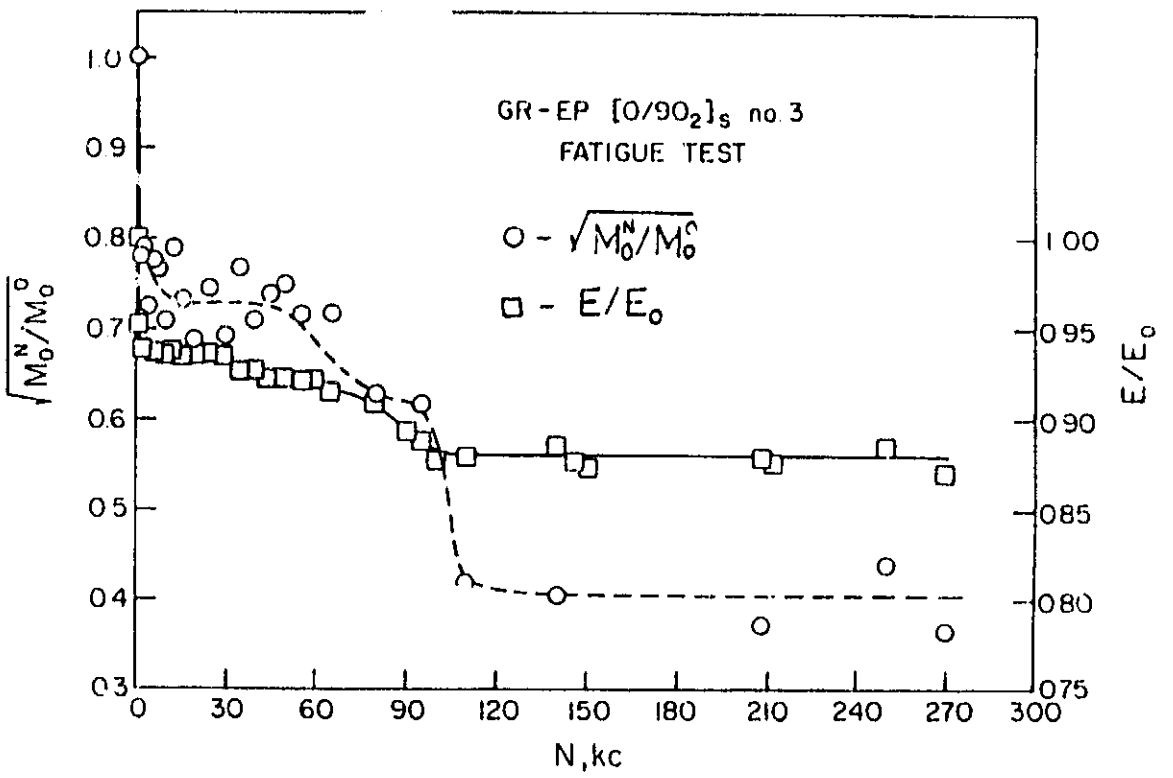

Fig. 35. Laminate stiffness (solid line) and root mean square of the frequency spectrum (dotted line) for fatigue test of a $[0,90_2]_s$ graphite epoxy specimen.

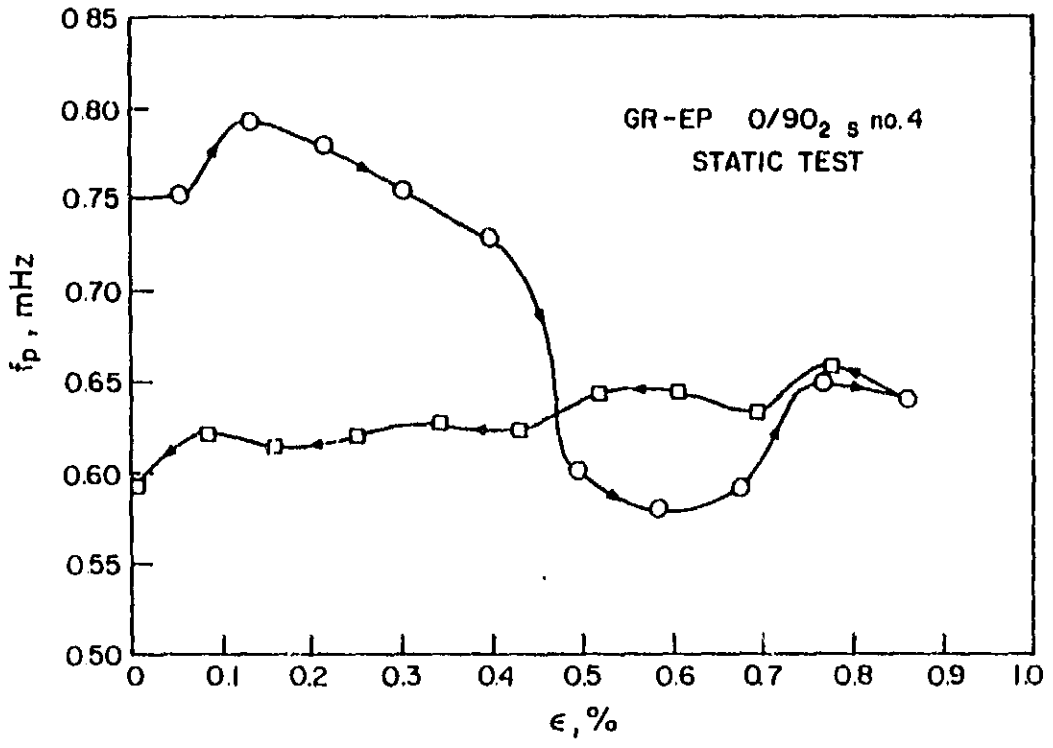

Fig. 36. Frequency of maxima in time doman, fp vs. strain for a static test of a $[0,90_2]_s$ graphite epoxy specimen.

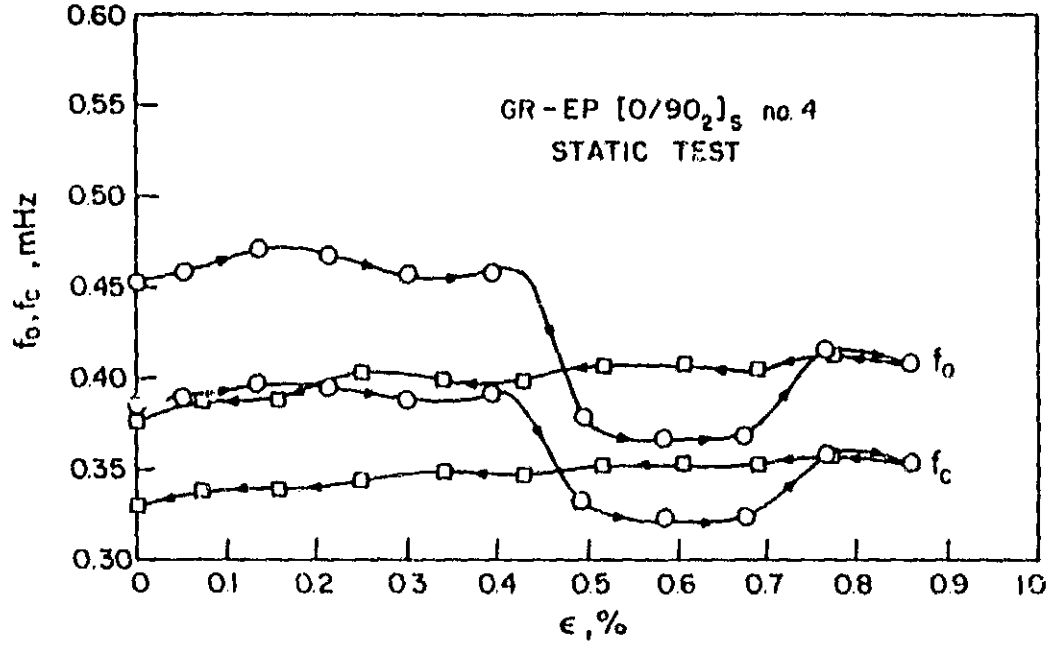

Fig. 37. Frequency of the mean value crossings, fo, and the location of the centroid fc, vs. strain for a static test of a $[0,90_2]_s$ graphite epoxy specimen.

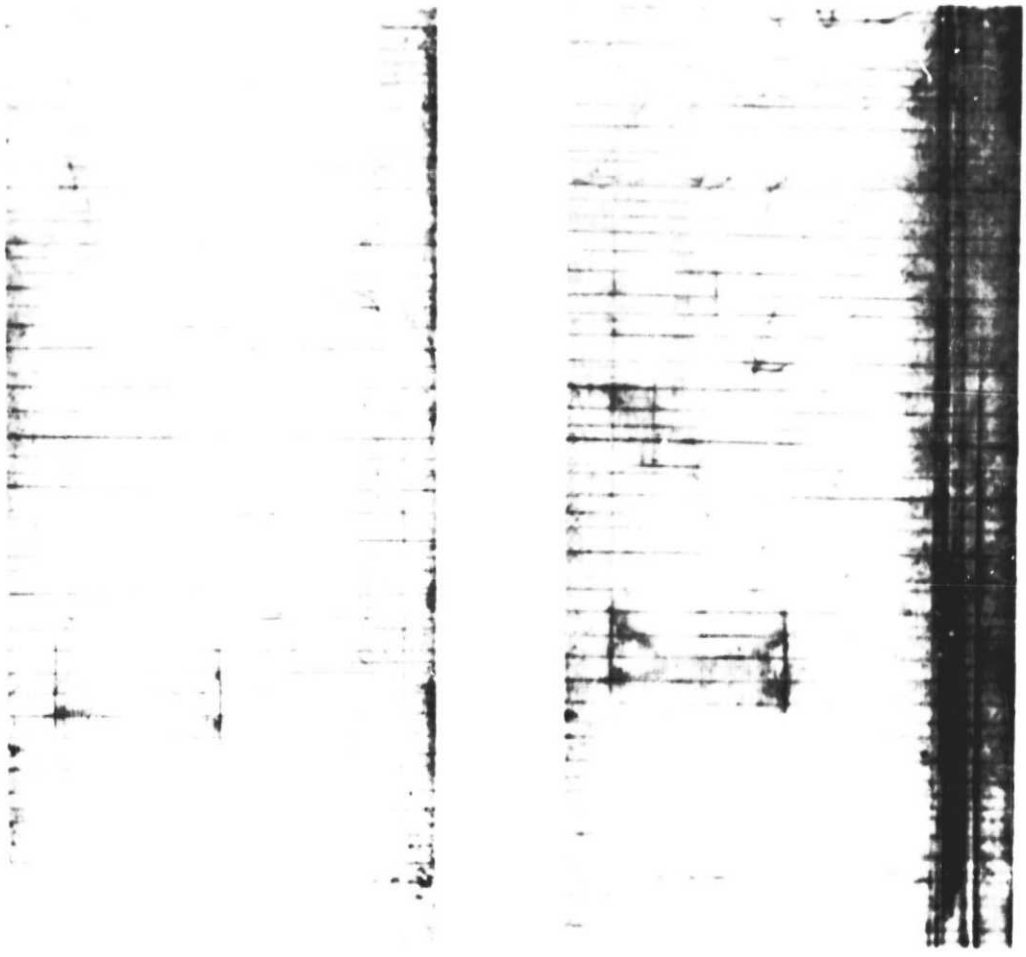

Fig. 38. Penetrant-enhanced radiograph showing (a) micro-delaminations and (b) macro-delaminations in a $[0,90_2]_s$ graphite epoxy specimen that has been cyclically loaded.

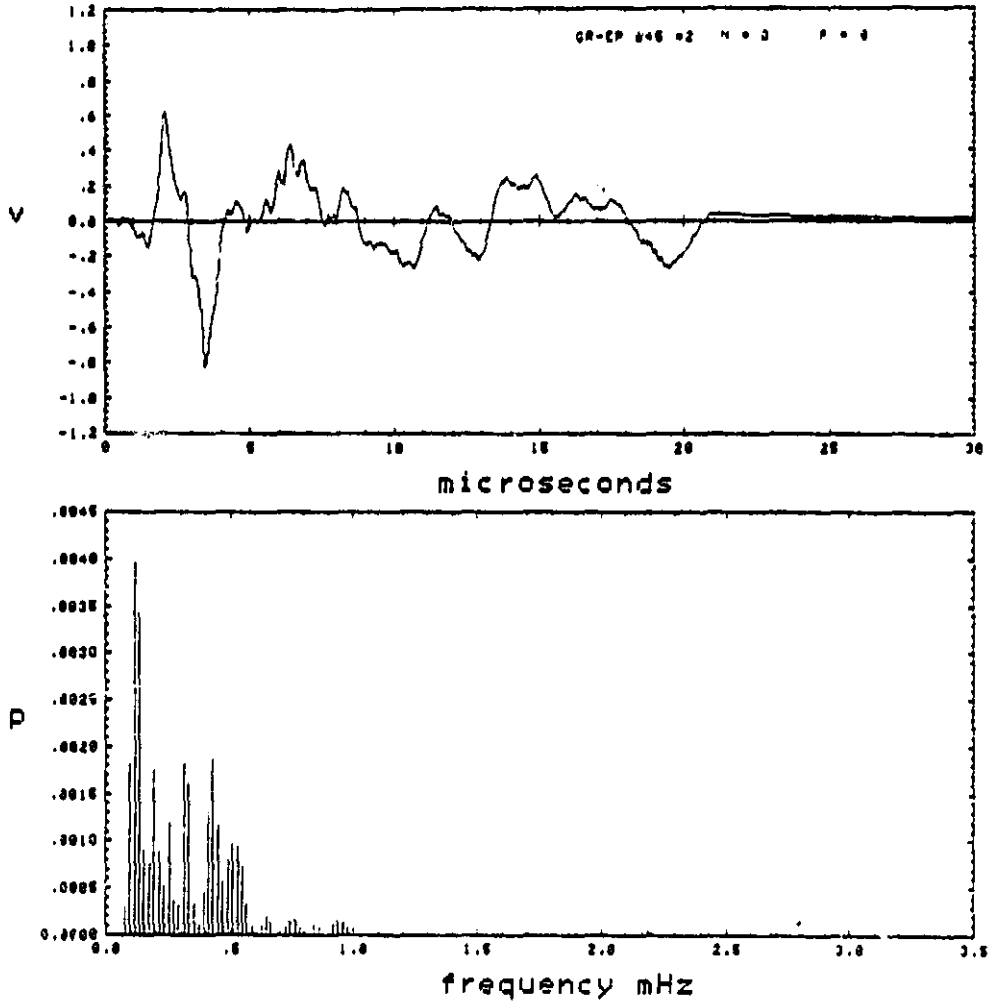

Fig. 39. The signal and its spectrum at N=0, P=0 for a $[0,\pm45]_s$ graphite epoxy specimen.

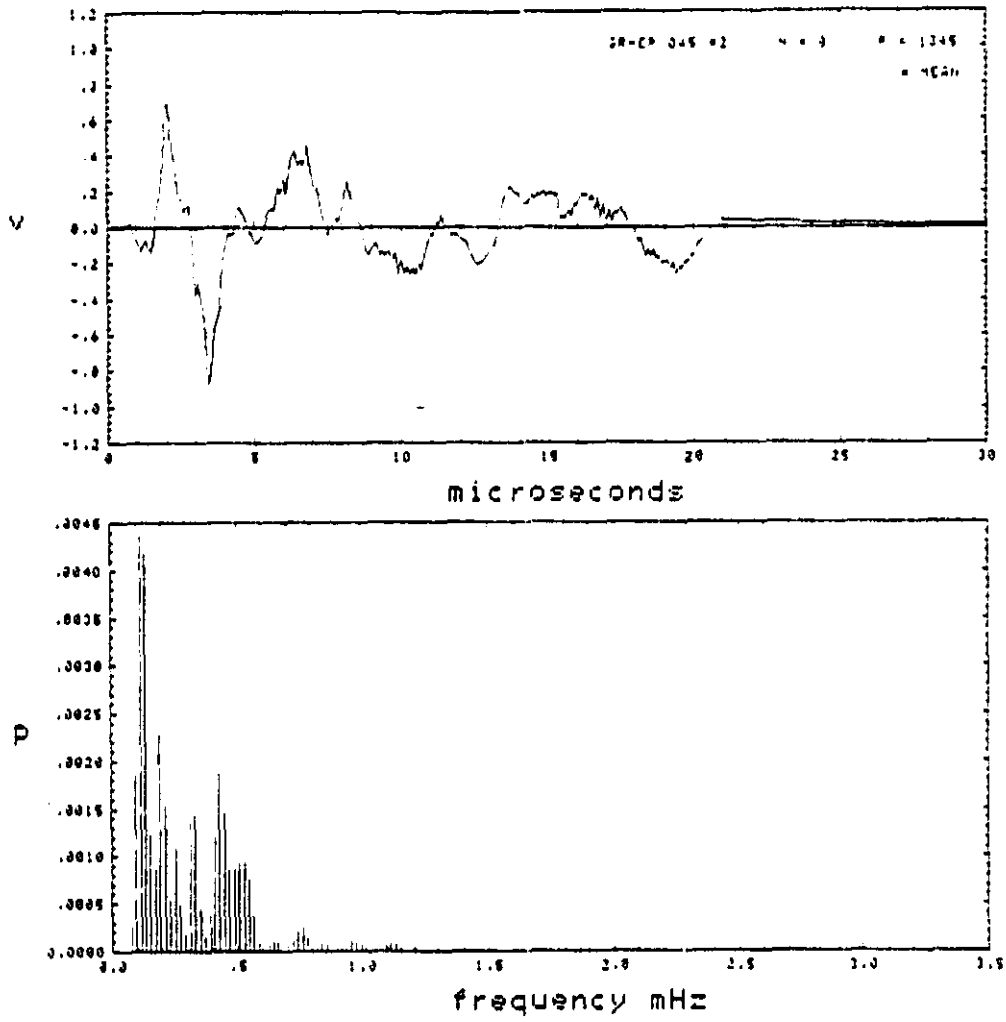

Fig. 40. The signal and its spectrum at N=1/2 P=1345 lbs for a $[0,\pm45]_s$ graphite epoxy specimen.

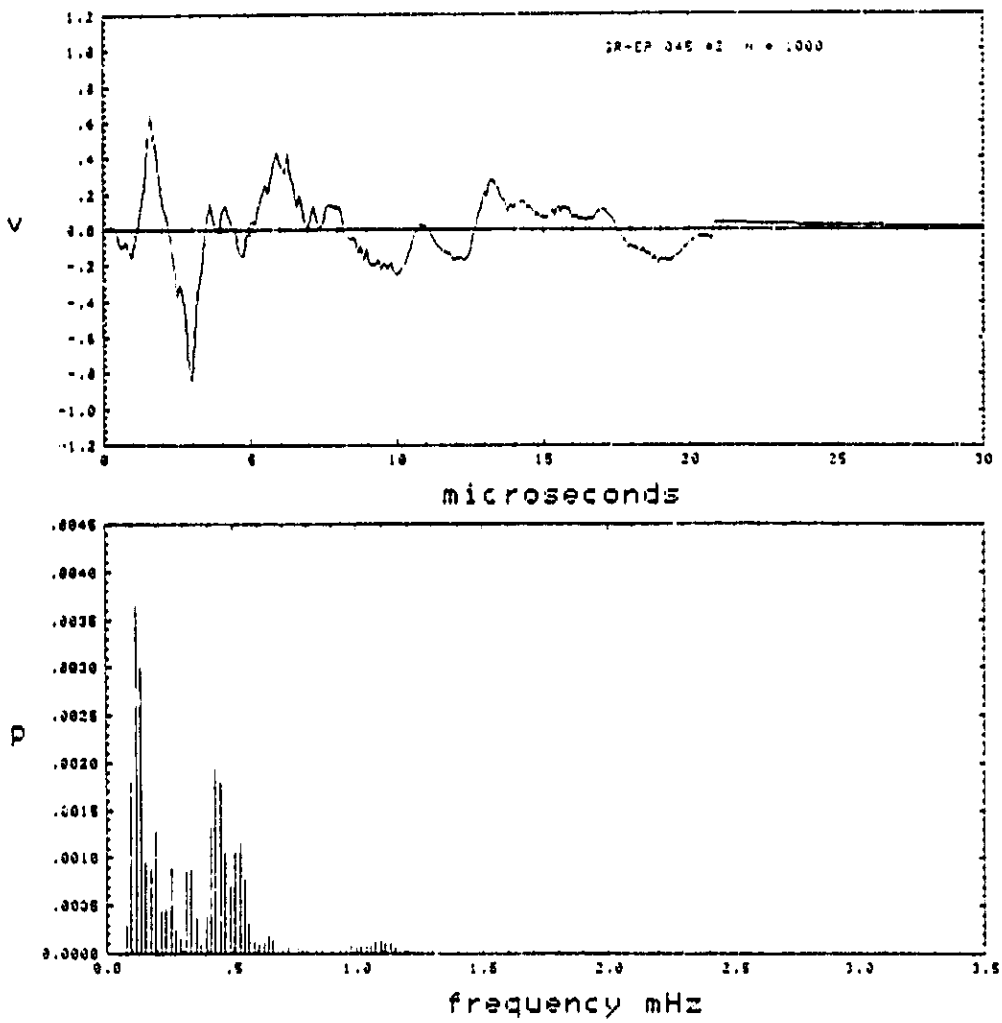

Fig. 41. The signal and its spectrum at N=1000, P=1345 lbs for a $[0,\pm45]_s$ graphite epoxy specimen.

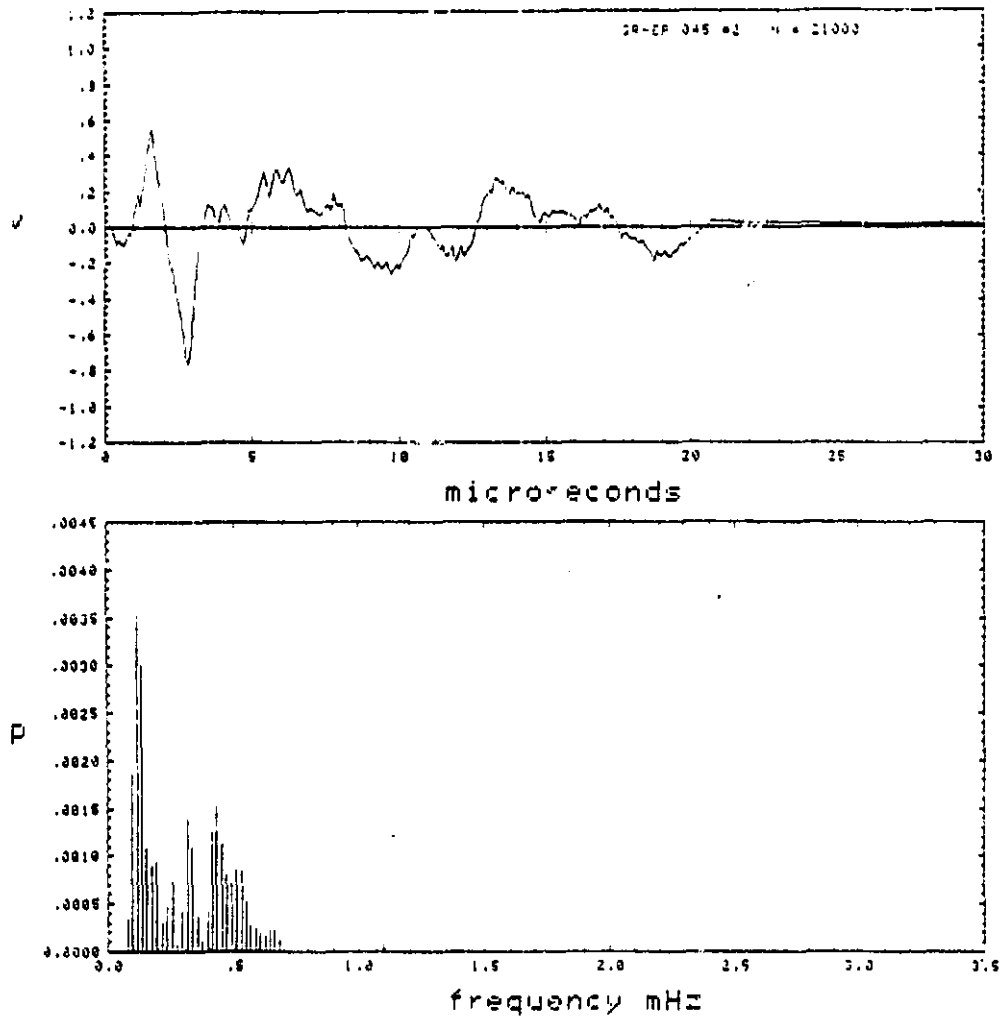

Fig. 42. The signal and its spectrum at N=21,000, P=1345 lbs for a $[0,\pm45]_S$ graphite epoxy specimen.

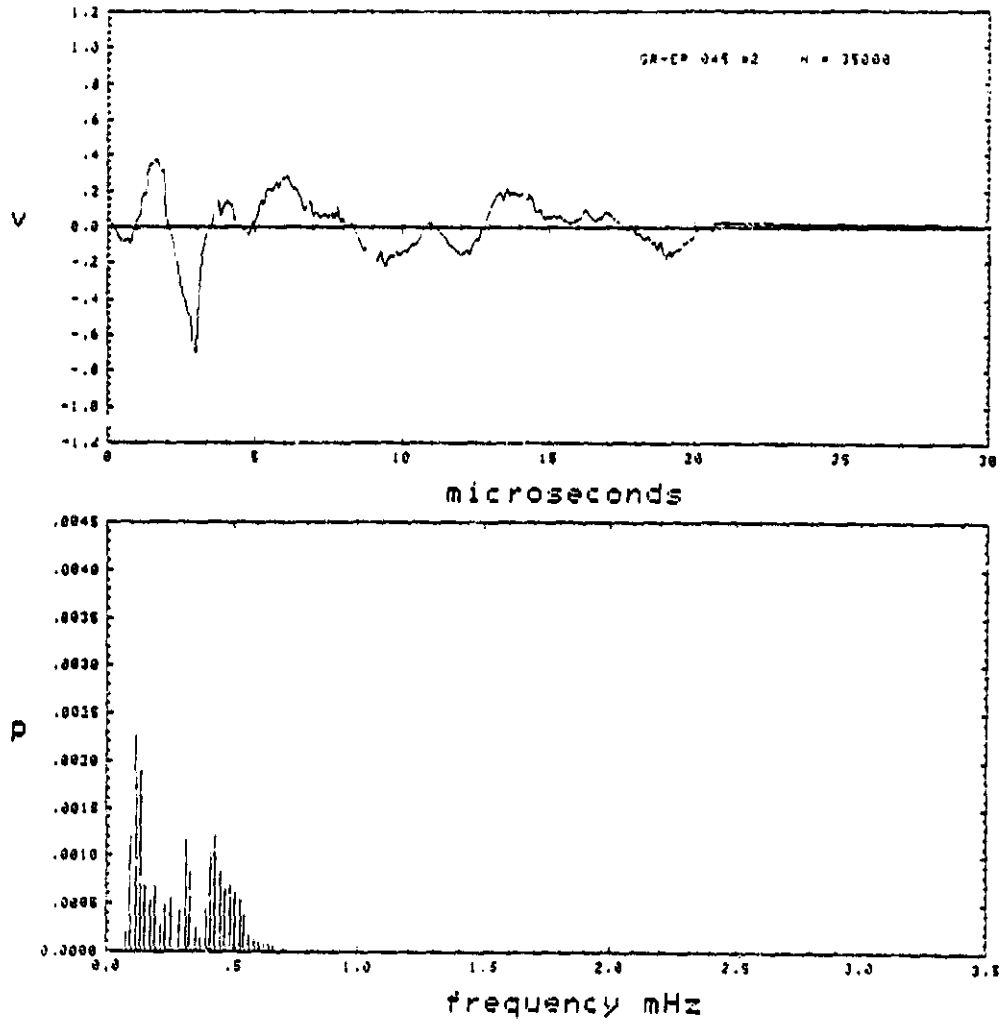

Fig. 43. The signal and its spectrum at N=35,000, P=1345 lbs for a $[0,\pm45]_s$ graphite epoxy specimen.

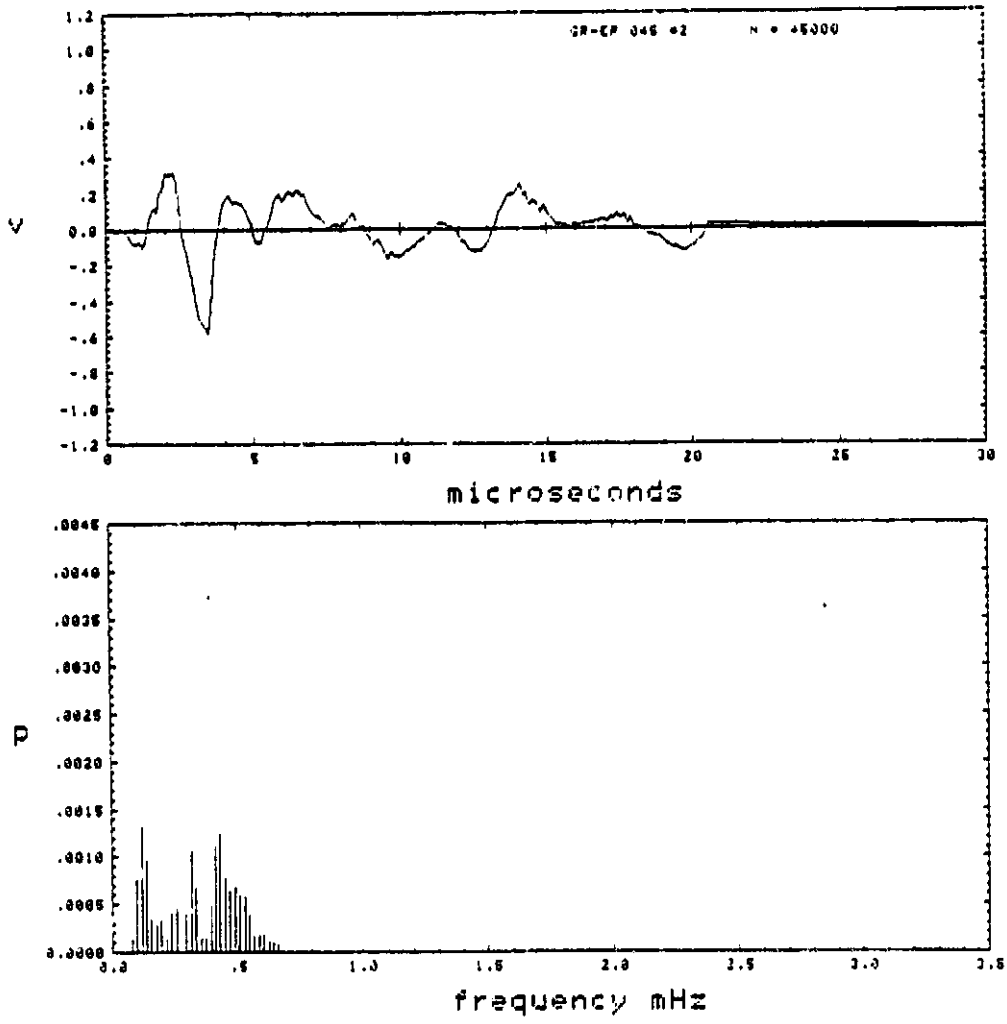

Fig. 44. The signal and its spectrum at N=45,000, P=1345 lbs for a $[0,\pm45]_s$ graphite epoxy specimen.

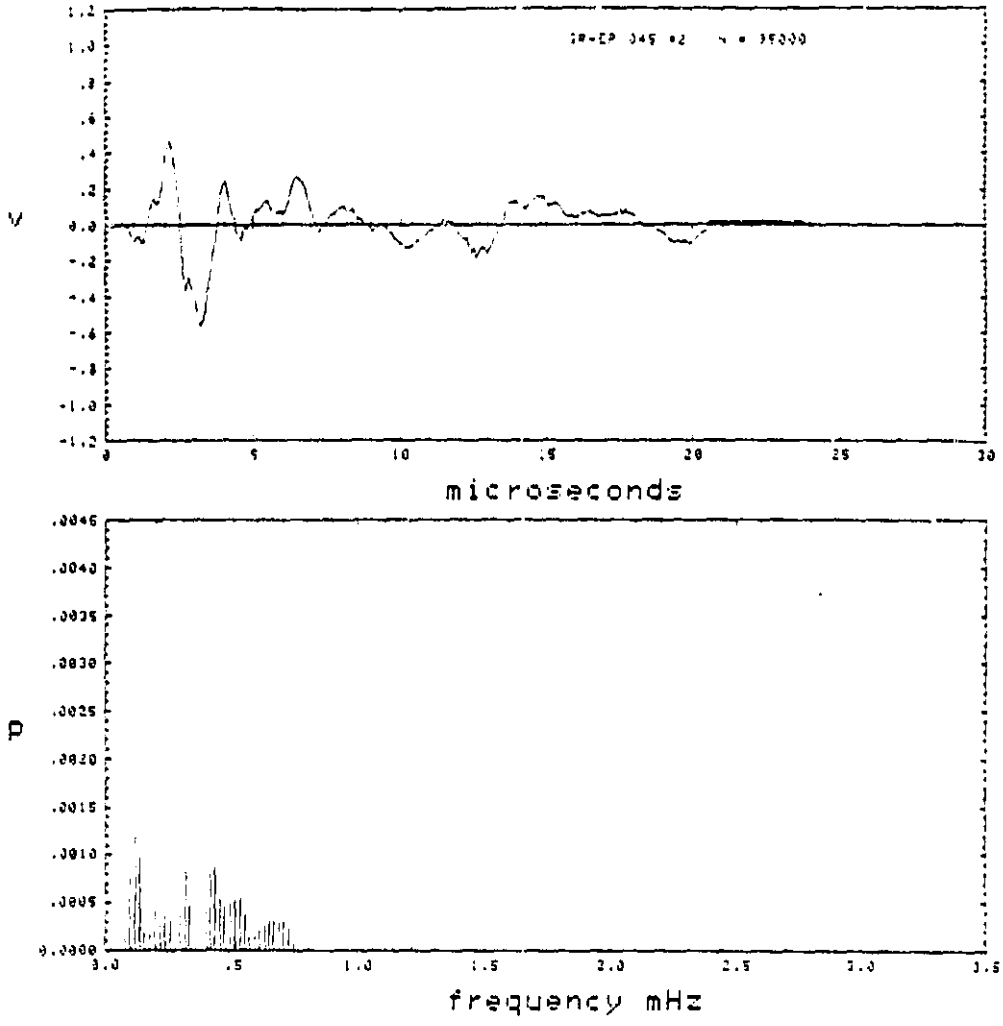

Fig. 45. The signal and its spectrum at N=95,000, P=1345 lbs for a $[0,\pm45]_S$ graphite epoxy specimen.

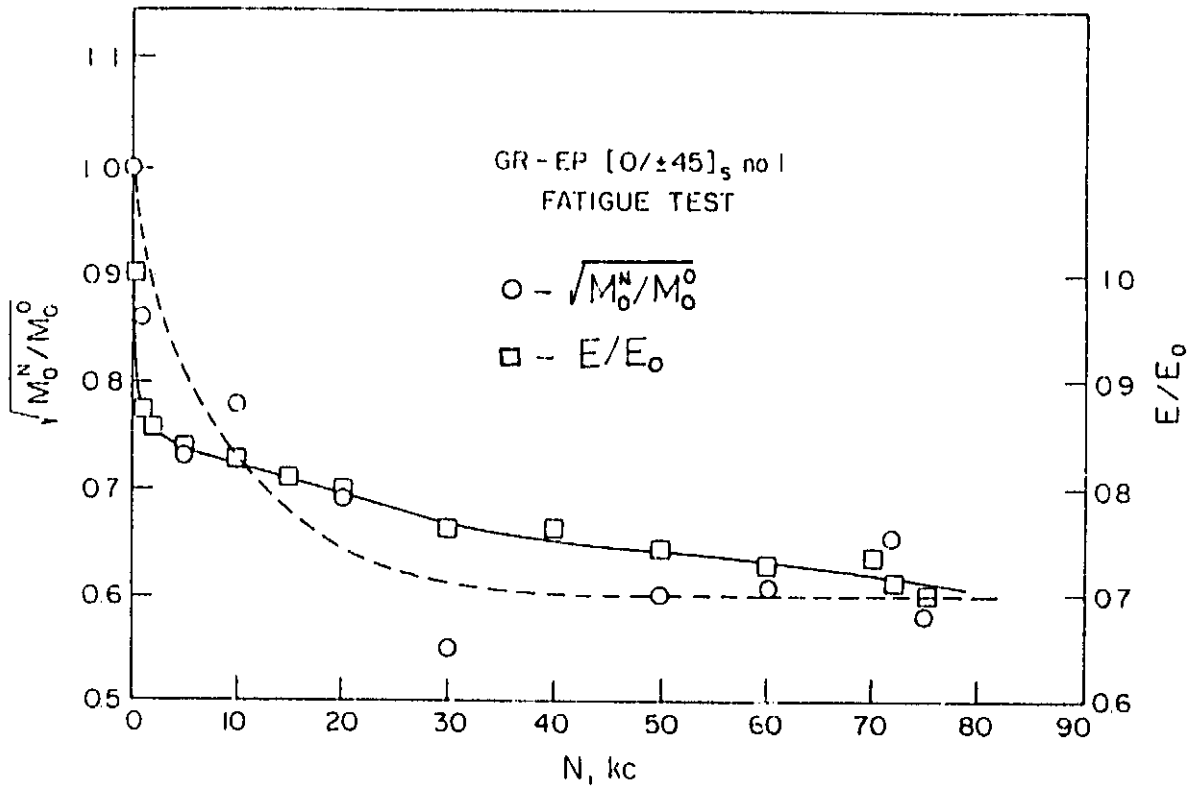

Fig. 46. Laminate stiffness (solid line) and root mean square of the frequency spectrum (dotted line) for fatigue test of a $[0,\pm45]_s$ graphite epoxy specimen.

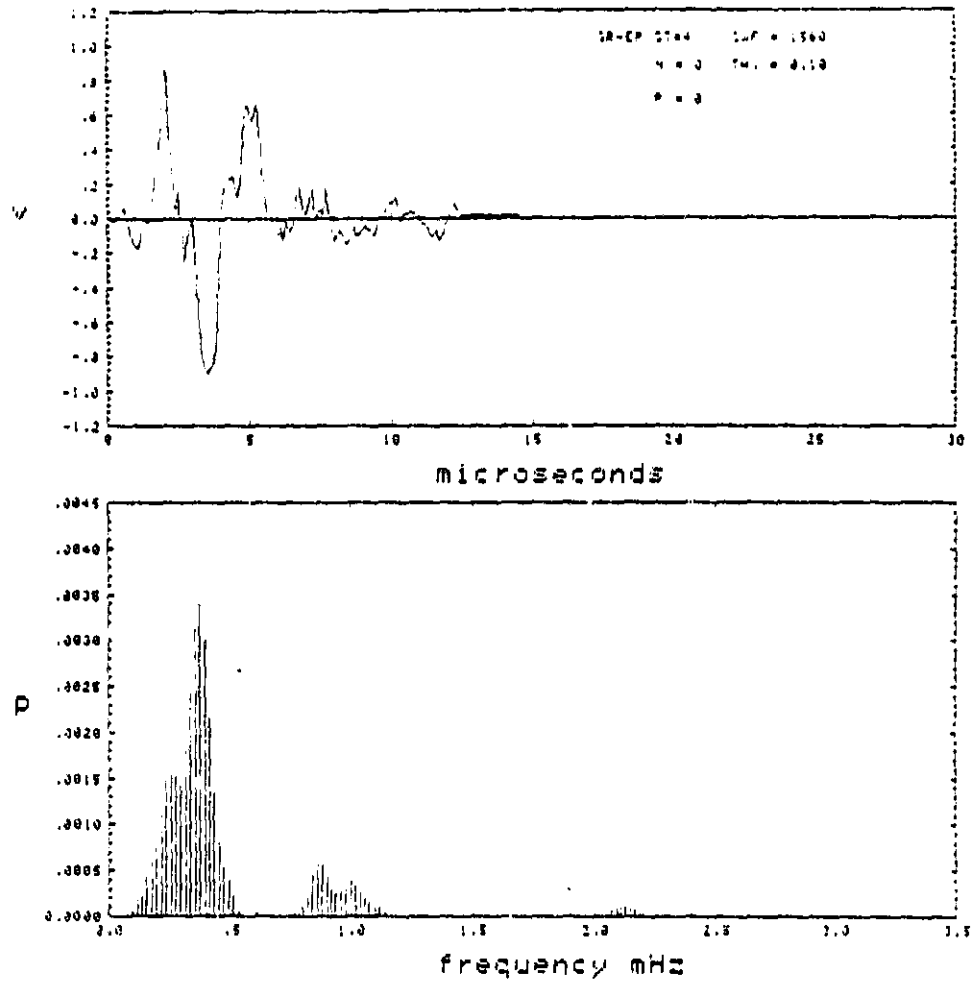

Fig. 47. The signal and its spectrum at N=0, P=0 for a $[0,90,\pm45]_S$ graphite epoxy specimen.

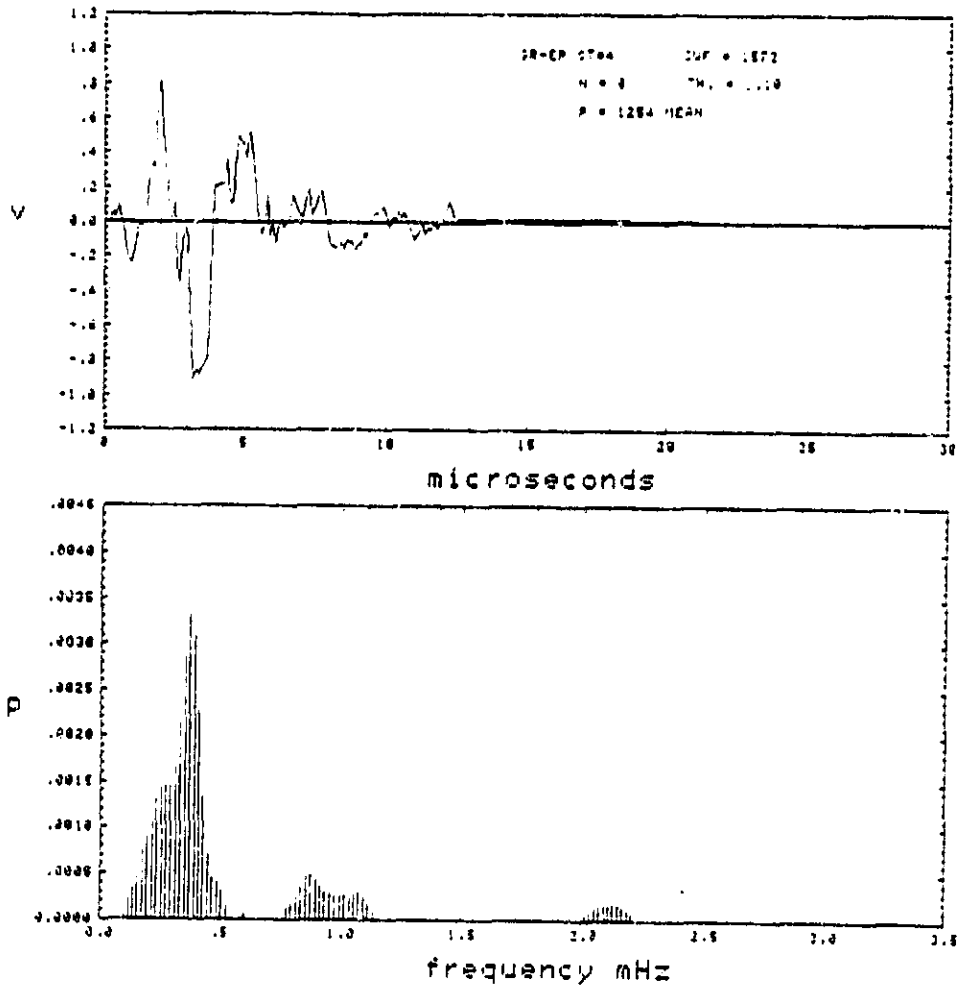

Fig. 48. The signal and its spectrum at N=½ P=1254 lbs for a $[0,90,\pm45]_S$ graphite epoxy specimen.

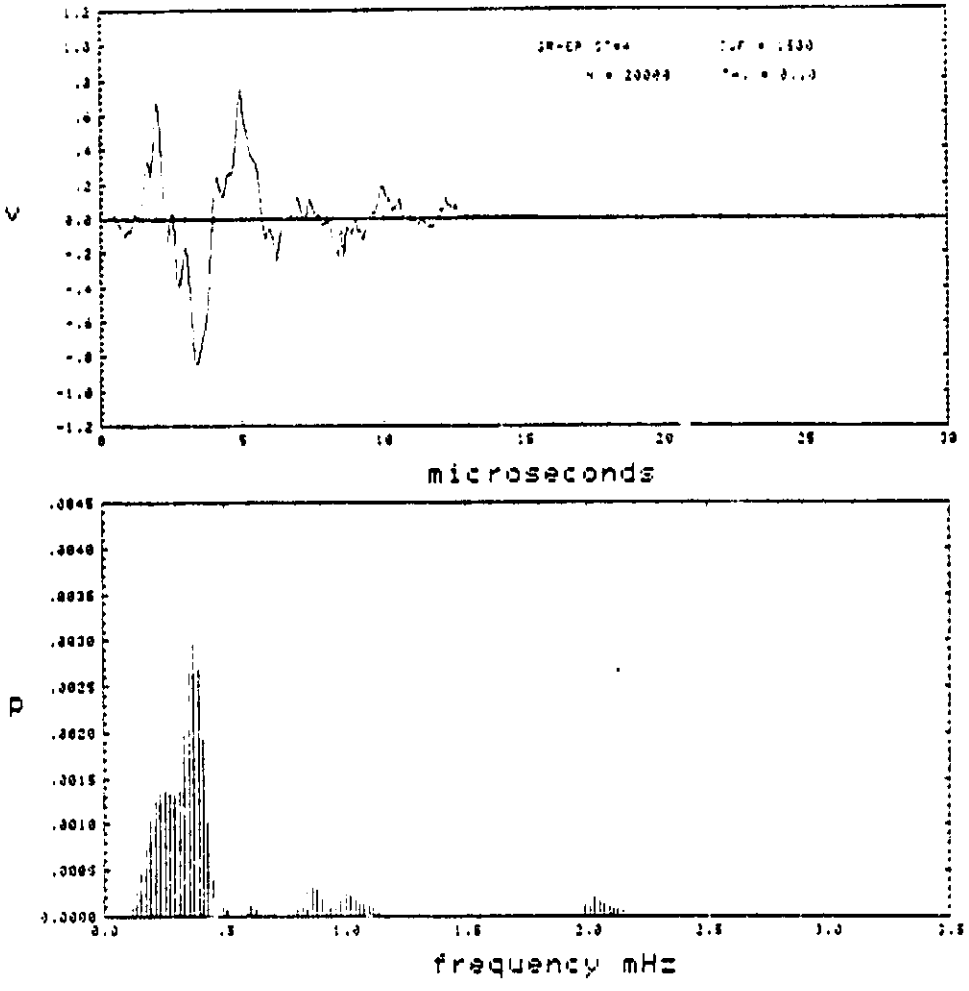

Fig. 49. The signal and its spectrum at N=20,000, P=1254 lbs for a $[0,90,\pm45]_S$ graphite epoxy specimen.

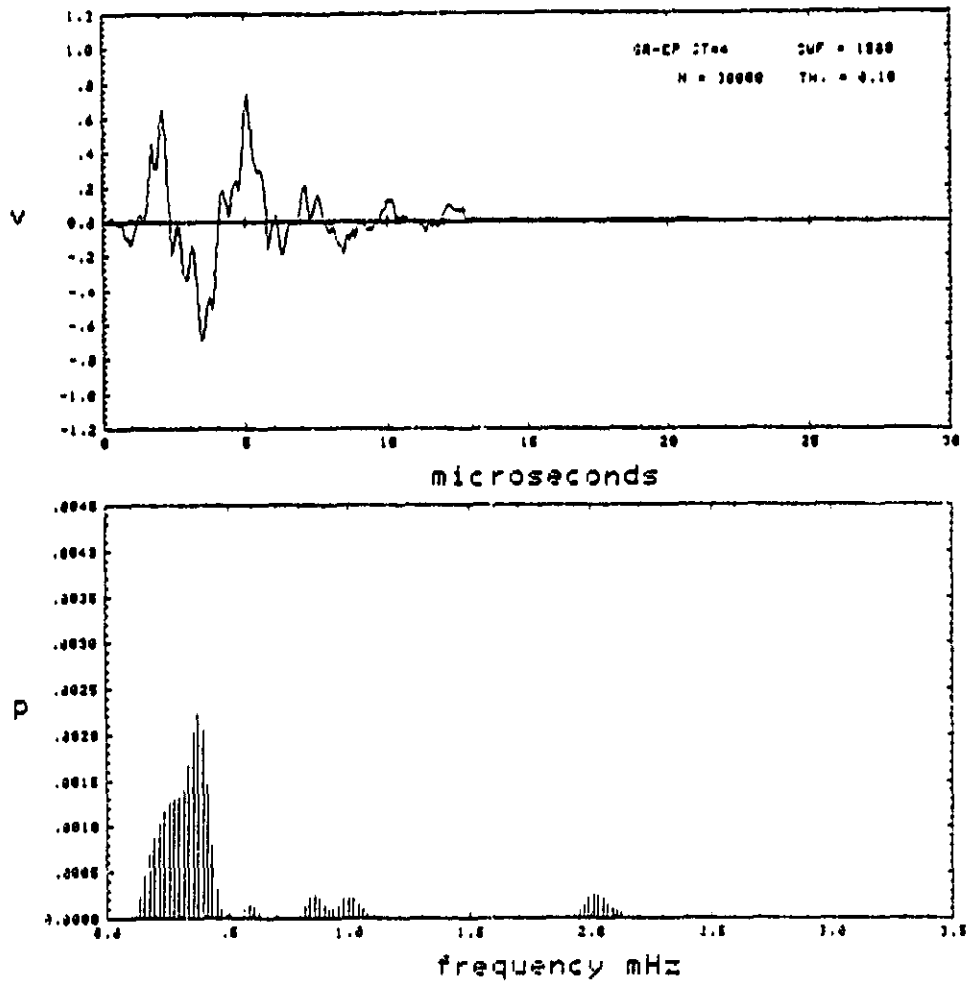

Fig. 50. The signal and its spectrum at N=30,000, P=1254 lbs for a $[0,90,\pm45]_s$ graphite epoxy specimen.

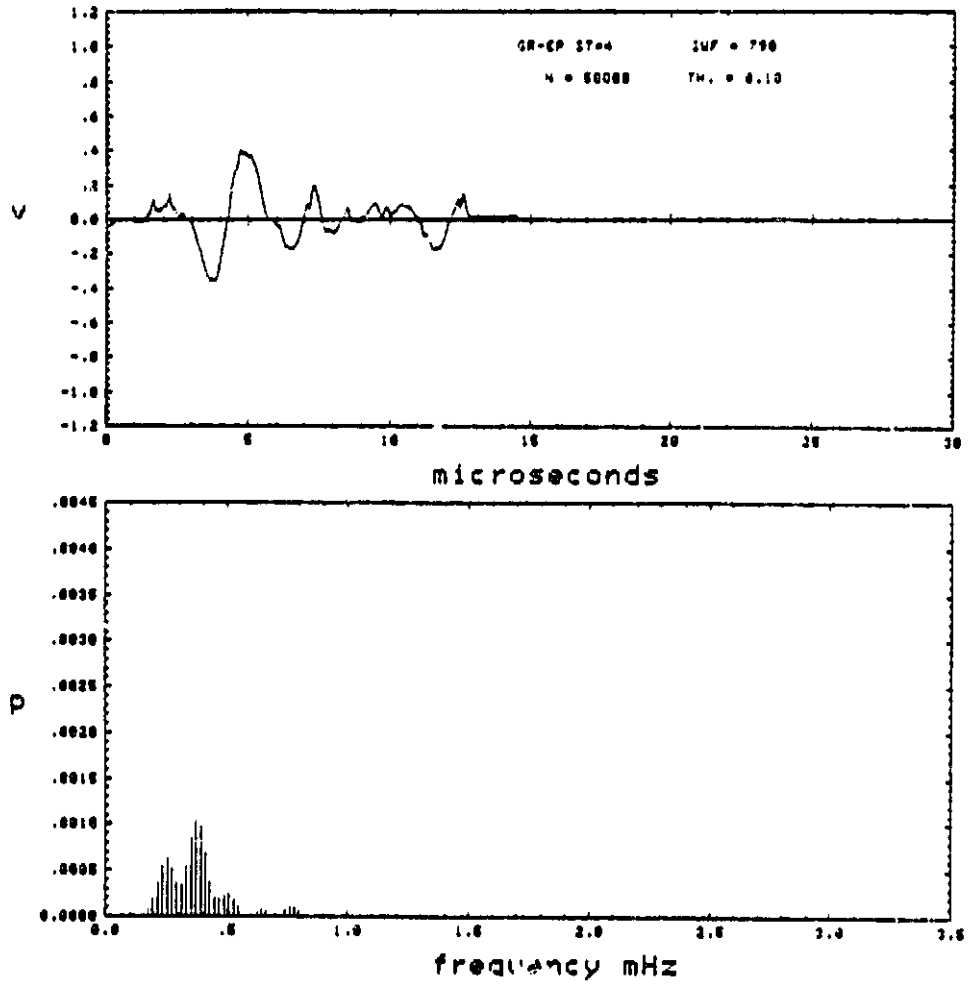

Fig. 51. The signal and its spectrum at N=50,000, P=1254 lbs for a $[0,90,\pm45]_s$ graphite epoxy specimen.

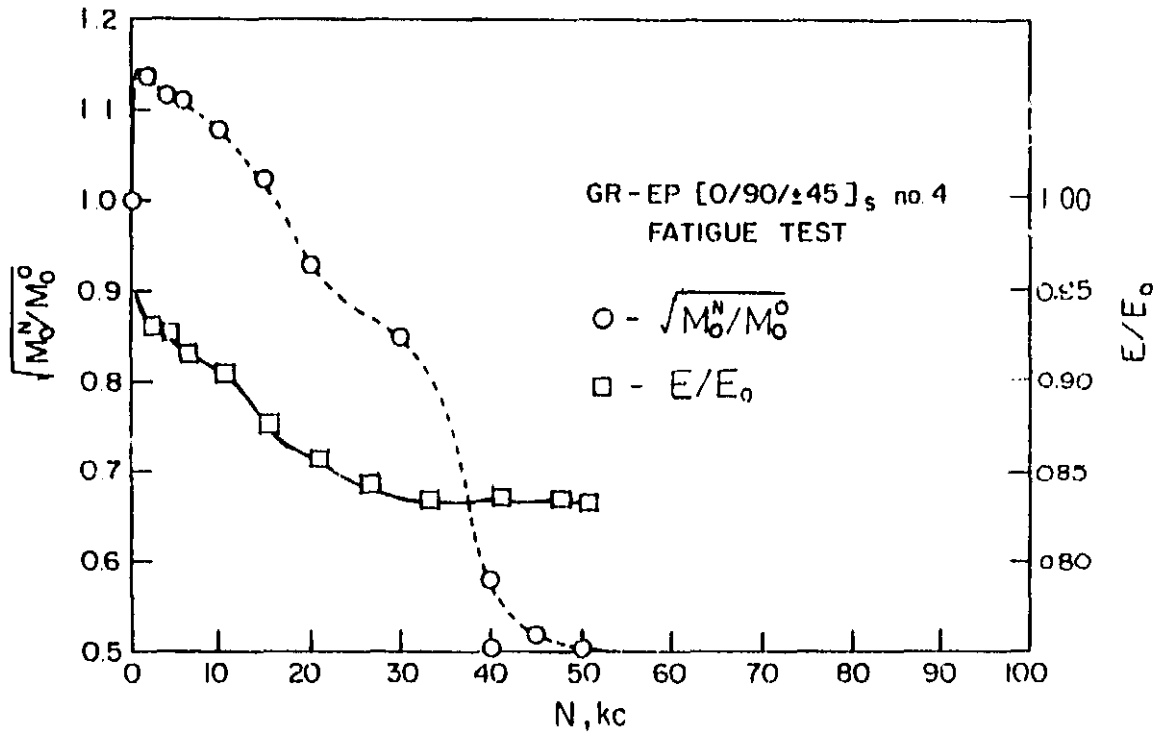

Fig. 52. Laminate stiffness (solid line) and root mean square of the frequency spectrum (dotted line) for fatigue test of a $[0,90,\pm45]_s$ graphite epoxy specimen.

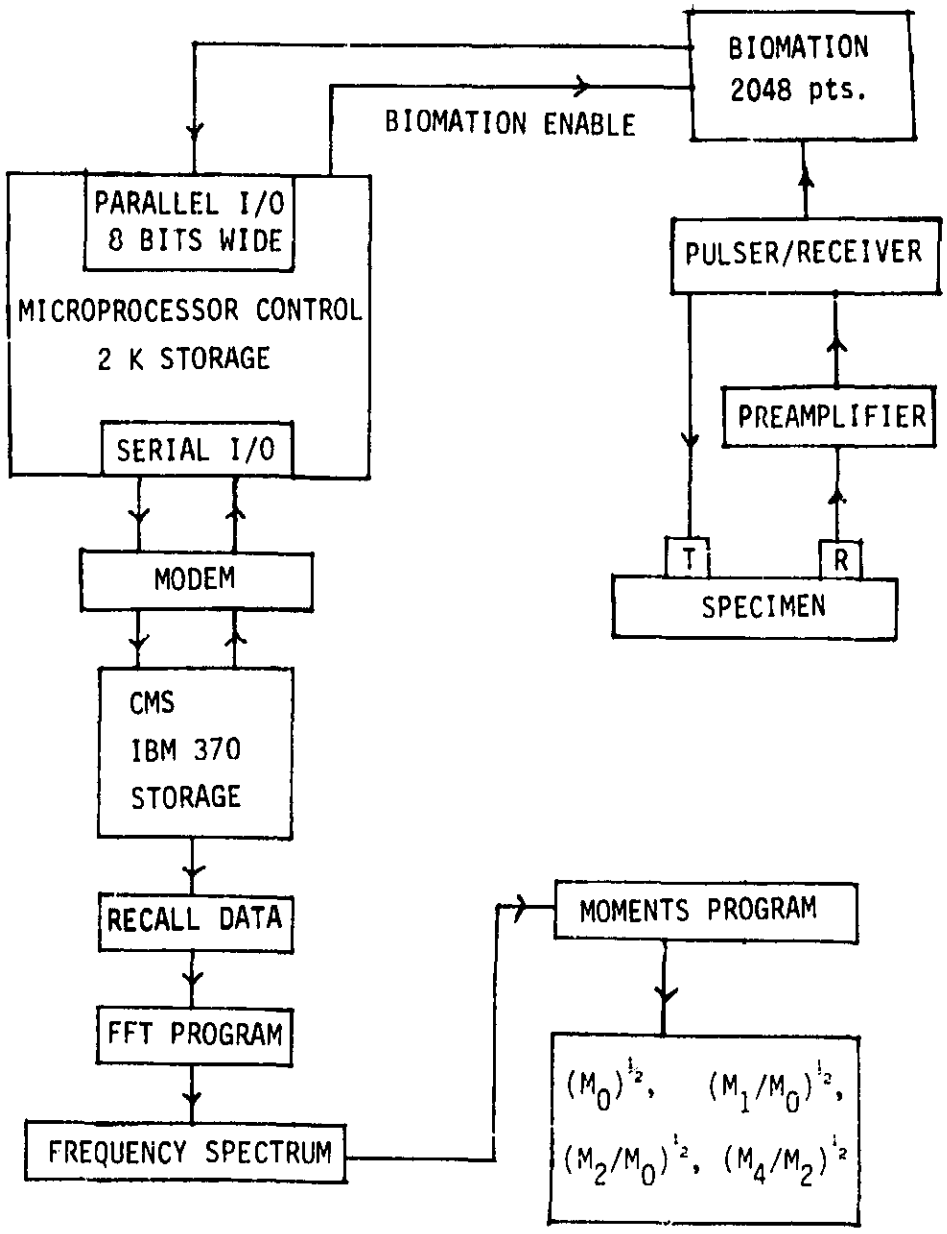

Fig. 53. Flow chart of the data acquisition and the moments evaluation system.

5. REFERENCES

1. R. Jamison and K. L. Reifsnider, "Effects of Defects in Composite Materials," to be published, ASTM.

2. R. Jamison, "Advanced Fatigue Damage Development in Graphite Epoxy Laminates," VPI & SU, PhD Dissertation, August 1982.

3. A. Vary and R. F. Clark, "Correlation of Fiber Composite Tensile Strength with the Ultrasonic Stress Wave Factor," NASA TM-78846, 1978.

4. E. Schreiber and O. L. Anderson, "Elastic Constants and Their Measurement," McGraw-Hill Book Co., 1973.

5. D. E. W. Stone and B. Clarke, "Ultrasonic Attenuation as a Measure of Void Content in Carbon Fiber Reinforced Plastics," Non-destructive Testing, Guildford, England, Vol. 8, no. 3, June 1975, pp. 137-145.

6. H. J. Sutherland and D. E. Munson, J. Comp. Matl's., Vol. 10, 1976, p. 118.

7. A. B. Schultz and D. N. Warwick, J. Comp. Matls., Vol. 5, 1971, p. 394.

8. E. G. Goeke and F. A. McClintock, J. Applied Phys., Vol. 46, 1975, p. 4671.

9. P. J. Cavano, "Resin/Graphite Fiber Composites," TRW-ER-7677F, TRW Equipment Labs, Dec. 1974.

10. A. Vary, "Concepts and Techniques for Ultrasonic Evaluation of Material Mechanical Properties," Mechanics of Nondestructive Testing, W. W. Stinchcomb, Editor, Plenum Press, 1980, pp. 123-141.

11. A. Vary and K. J. Bowles, "Use of an Ultrasonic-acoustic Technique for Nondestructive Evaluation of Fiber Composite Strength," NASA TM-73813, 1978.

12. A. Vary and K. J. Bowles, "Ultrasonic Evaluation of the Strength of Unidirectional Graphite-Polyimide Composites," NASA TM-X-73646, 1977.

13. D. R. Hull and A. Vary, "Interrelation of Material Microstructure, Ultrasonic Factors, and Fracture Tougnness of a Two Phase Titanium Alloy," NASA TM-82810, 1982.

14. J. H. Williams and N. R. Lampert, "Ultrasonic Evaluation of Impact-damaged Graphite Fiber Composites," Materials Evaluation, Vol. 38, Dec. 1980, pp. 68-72.

15. E. G. Henneke, II, J. C. Duke, Jr., W. W. Stinchcomb, A. Govada and A. Lemascon, "A Study of the Stress Wave Factor Technique for the Characterization of Composite Materials," NASA CR 3670.

16. A. Govada and J. C. Duke, Jr., "Application of Ultrasonics to Damage Development in Metal Matrix Composites," ASNT Paper Summaries, 1982, pp. 379-385.

17. J. C. Duke, Jr., E. G. Henneke, II, W. W. Stinchcomb and K. L. Reifsnider, "Characterization of Composite Materials by Means of the Ultrasonic Stress Wave Factor," Composite Structures 2, I. H. Marshall, Editor, Applied Scientific Publishers, 1983, pp. 53-60.

18. D. T. Hayford and E. G. Henneke, II, "A Model for Correlating Damage and Ultrasonic Attenuation in Composites," ASTM STP 647, 1979, pp. 184-200.

19. D. M. Egle and A. E. Brown, J. Acoust. Society Am., Vol. 57, 1975, p. 591.

20. D. M. Egle and A. E. Brown, J. Test. Eval., Vol. 4, 1976, p. 196.

21. L. J. Graham and G. A. Alers, "Monitoring Structural Integrity by Acoustic Emission," ASTM Special Technical Publication 571, Philadelphia, PA, 1975, p. 11.

22. D. Post, "Optical Interference for Deformation Measurements -- Classical, Holographic and Moire Interferometry," Mechanics of Nondestructive Testing, W. W. Stinchcomb, Editor, Plenum Press, 1980, pp. 1-53.

23. R. Talreja, "On Fatigue Life Under Stationary Gaussian Random Loads," Engineering Fracture Mechanics, Vol. 5, 1973, pp. 993-1007.

24. S. O. Rice, "Mathematical Analysis of Random Noise," Bell Systems Technical Journal, 23, 1944.

25. IMSL Subroutine, FFTRC, VA Tech Computing Center, VPI & SU, Blacksburg, VA.

26. R. Talreja, Private communication, March 1984.

APPENDIX A

Moiré interferometry depends upon diffraction of light as well as interference [ ]. Moire fringes are obtained by using diffraction gratings. A grating is a surface with regularly spaced bars or furrows. The distance between two consecutive bars is called pitch, g. Frequency f of a grating is the number of bars per unit length

$$f = \frac{1}{g}$$

A grating divides every incident wavetrain into a multiplicity of wavetrains of smaller intensities; and it causes these wavetrains to emerge in certain preferred directions. A parallel beam incident at a particular angle on the grating divides it into a series of beams that emerge at preferred angles. These beams are called diffraction orders and are numbered in sequence beginning with the zero order, which is the mirror reflection of the incident beam. The angle between the neighboring diffraction orders is small for a coarse grating and it is large

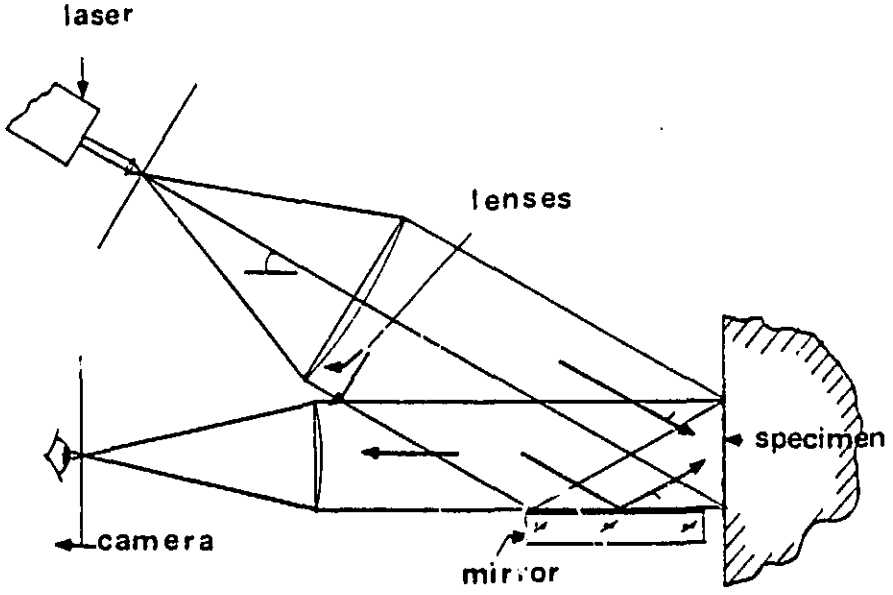

Figure a. - Schematic of moiré interferometry setup.

for a fine grating.

The grating equation defines the angles of diffraction, viz.,

$\sin \theta = m\lambda + \sin \alpha$

where m defines the diffraction order of the beam under consideration.

Coarse moiré is produced by the superposition of two coarse gratings with frequencies in the range of about 1 to 40 lines/mm. One of them is an active grating (glued to the surface of the specimen) and the other a reference grating (virtual). The virtual grating is formed by the intersection of the wavetrains from the reflective active grating and a mirror beside the active grating. Fig. a shows the moiré interferometry set up.

Moiré fringes are the locus of points of constant displacements, specifically the in-plane displacement component in the direction perpendicular to the lines of the reference grating [22]. Moiré fringe order, N, denotes the number of cycles of intensity fluctuation experienced at any point as the displacement changes from zero to its final value.

$u = g N_x$; x = longitudinal direction

$v = g N_y$; y = transverse direction

--u,v are displacements in the longitudinal and transverse directions

--g = pitch of the reference grating

--N_x, N_y are the fringe orders when lines on the reference grating are perpendicular to the longitudinal and the transverse directions, respectively.

From the displacements we can get strains

$$\varepsilon_x = \frac{du}{dx}$$

$$\varepsilon_y = \frac{dv}{dy}$$

$$r_{\gamma y} = \frac{du}{dy} + \frac{dv}{dx}$$

where ε_x and ε_y are the normal strains and $\gamma_{\gamma y}$ is the shear strain. Stresses can be determined using stress-strain relationships. Since the strains and the associated displacements are very small, gratings of fine pitch and high frequency are required [22].

A grating is made by exposing a high-resolution photographic plate to two intersecting beams of coherent light. Frequency of the grating is controlled by the angle of intersection according to

$$\text{Sin } \alpha = \frac{\lambda}{\alpha} f$$

where α = incident angle

λ = wavelength of light used

f = frequency of grating

The two intersecting beams give rise to a diffraction pattern of light and dark bands. When the plate is developed silver grains remain in the exposed zones, while the silver is leached out in the unexposed zones. The gelatin matrix shrinks upon drying, but since it is partially restrained by the silver, shrinkage is greatest in the unexposed zones. The result is a plate with a furrowed surface which can be used as a grating. The grating is mirrorized with aluminum to improve its reflective qualities. The grating is then transferred and attached to the specimen with an adhesive.

APPENDIX B

Computer Program

```
//B1225PUT JOB 11992,PASI,REGION=250K,TIME=(0,59),MSGLEVEL=(0,0)
/*PRIORITY IDLE
/*JOBPARM LINES=100,CARDS=100
//STEP1 EXEC FORTXCGV
//FORT.SYSPRINT DD DUMMY
//FORT.SYSIN DD *
C$JOB           ANIL,PAGE=20
      IMPLICIT REAL*8(A-H,O-Z)
      INTEGER N,IWK(11),IA(2048)
      REAL    AI(2048),WK(1),AMP(1025)
      COMPLEX X(1025)
C
C     ..................VOL=INPUT VOLTAGE RANGE .....................
C
      DATA PI,VOL,DELX/3.141592654D0,2.0D0,0.05D0/
      N=2048
      NNH=N/2+1
      TOTAL=N*DELX
      READ 100,(IA(I),I=1,N)
      DO 10 KK=1,N
      AI(KK)=0.0
      AI(KK)=IA(KK)
      IF(AI(KK).GT.127.0)AI(KK)=AI(KK)-256.0
 10   AI(KK)=VOL*AI(KK)/128.0
C10   AI(KK)=VOL*(AI(KK,-128.0)/128.0
      PRINT 202
      DX=0.0D0
      DO 20 IJ=1,N
      PRINT 110,DX,AI(IJ)
 20   DX=DX+DELX
C
      CALL FFTRC(AI,N,X,IWK,WK)
C
C     PRINT 110,(X(I),I=1,NNH)
C
      PRINT 201
      DO 30 I=1,NNH
      AMP(I)=0.0
      FN=2.0*PI*I/TOTAL
      AMP(I)=CABS(X(I))
 30   PRINT 110, FN,AMP(I)
C ..... THE FOLLOWING IS FOR CALCULATING THE MOMENTS ..................
      NM=NNH-1
      FNT=2.0*PI*NNH/TOTAL
      AM0=0.0
      AM1=0.0
      AM2=0.0
      AM4=0.0
      DO 40 I=1,NM
      AM0=AM0+(AMP(I+1)-AMP(I))*FNT/2.0
      AM1=AM1+(AMP(I+1)-AMP(I))*FNT/2.0 * ((I-1)*FNT + FNT/2.0)
      AM2=AM2+(AMP(I+1)-AMP(I))*FNT/2.0 * ((I-1)*FNT + FNT/2.0)**2
 40   AM4=AM4+(AMP(I+1)-AMP(I))*FNT/2.0 * ((I-1)*FNT + FNT/2.0)**4
      A=DSQRT(DABS(AM0))
      B=AM1/AM0
      C=DSQRT(DABS(AM2/AM0))
      D=DSQRT(DABS(AM4/AM2))
      PRINT 130,A,B,C,D
C
 100  FORMAT(I3,17I4)
 110  FORMAT(2E15.5)
 120  FORMAT(E15.5)
 130  FORMAT(/,' SQUARE ROOT OF M0=',E15.5,/,' M1 OVER M0=',E15.5,/,
     *       ' SQUARE ROOT OF M2 OVER M0=',E15.5,/,
     *       ' SQUARE ROOT OF M4 OVER M2=',E15.5,/)
 201  FORMAT(/,'FREQUENCY VS AMPLITUDE',/)
 202  FORMAT(/,'TIME VS VOLTAGE',/)
      STOP
      END
//GO.SYSIN     DD *
```

1. Report No.	2. Government Accession No	3. Recipient's Catalog No
NASA CR-174870		

4. Title and Subtitle	5. Report Date
A Study of the Stress Wave Factor Technique for the Characterization of Composite Materials	February 1985
	6. Performing Organization Code

7. Author(s)	8. Performing Organization Report No.
A.K. Govada, J.C. Duke, Jr., E.G. Henneke II, and W.W. Stinchcomb	CCMS-84-13
	10. Work Unit No

9. Performing Organization Name and Address	11. Contract or Grant No.
Virginia Polytechnic Institute and State University Blacksburg, Virginia 24061	NAG 3-172
	13. Type of Report and Period Covered
12. Sponsoring Agency Name and Address	Contractor Report
National Aeronautics and Space Administration Washington, D.C. 20546	14. Sponsoring Agency Code 505-36-22

15. Supplementary Notes

Final report. Project Manager, Alex Vary, Structures Division, NASA Lewis Research Center, Cleveland, Ohio 44135.

16. Abstract

This study has investigated the potential of the Stress Wave Factor as an NDT technique for thin composite laminates. The conventional SWF and an alternate method for quantifying the SWF were investigated. Agreement between the initial SWF number, ultrasonic C-scan, inplane displacements as obtained by full field moiré interferometry, and the failure location have been observed. The SWF number was observed to be the highest when measured along the fiber direction and the lowest when measured across the fibers. The alternate method for quantifying the SWF used square root of the zeroth moment ($\sqrt{M_0}$) of the frequency spectrum of the received signal as a quantitative parameter. When $[0,90_2]_s$, $[0,\pm45]_s$ and $[0,90,\pm45]_s$ graphite epoxy laminates were cyclically loaded, $\sqrt{M_0}$ decreased with the number of cycles. Decreases in the amplitudes of the higher harmonics of the frequency spectrum occurred as a result of transverse matrix cracking in the 90^0 plies of the laminates. The decreases in $\sqrt{M_0}$ were in agreement with the reduction in laminate stiffness due to cyclic loading. The decreases in $\sqrt{M_0}$ were larger than the reduction in the laminate stiffnesses due to cyclic loading. From this study it therefore appears that the stress wave factor has an excellent potential to monitor damage development in thin composite laminates.

17. Key Words (Suggested by Author(s))	18. Distribution Statement
Nondestructive testing; Acousto-ultrasonics; Fiber reinforced composites; Mechanical properties; Damage; Strength; Stiffness	Unclassified - unlimited STAR Category 38

19. Security Classif. (of this report)	20. Security Classif. (of this page)	21. No. of pages	22. Price*
Unclassified	Unclassified	102	A06

*For sale by the National Technical Information Service, Springfield, Virginia 22161